EARLY BRAIN TISSUE REACTION SURROUNDING MICHIGAN-STYLE MICROELECTRODE ARRAYS INDICATES THAT EXTENSIVE REMODELING OF GLIAL AND NEURONAL POPULATIONS OCCURS DURING THE FOREIGN BODY RESPONSE

by

Amanda L. Pollock

A thesis submitted to the faculty of
The University of Utah
in partial fulfillment of the requirements for the degree of

Master of Science

Department of Bioengineering

The University of Utah

May 2007

THE UNIVERSITY OF UTAH GRADUATE SCHOOL

SUPERVISORY COMMITTEE APPROVAL

of a thesis submitted by

Amanda L. Pollock

This thesis has been read by each member of the following supervisory committee and by majority vote has been found to be satisfactory.

12/21/06 Chair: Patrick A. Tresco

12/21/06 Richard A. Normann

12.21.06 Patrick F. Kiser

THE UNIVERSITY OF UTAH GRADUATE SCHOOL

FINAL READING APPROVAL

To the Graduate Council of the University of Utah:

I have read the thesis of Amanda L. Pollock in its final form and have found that (1) its format, citations, and bibliographic style are consistent and acceptable; (2) its illustrative materials including figures, tables, and charts are in place; and (3) the final manuscript is satisfactory to the supervisory committee and is ready for submission to The Graduate School.

1/17/07
Date

Patrick A. Tresco
Chair: Supervisory Committee

Approved for the Major Department

Richard D. Rabbitt
Chair/Dean

Approved for the Graduate Council

David S. Chapman
Dean of The Graduate School

ABSTRACT

Previous studies indicate that the brain tissue reaction to implanted silicon recording microelectrode arrays involves hyperplasia of macrophages, microglia and astrocytes, and that these reactions are accompanied by a decrease in the density of neurons immediately surrounding the implant. It is generally believed that the foreign body response is a major factor in the inconsistent recording performance observed with these devices. To gain insight into the earliest events, we used immunohistochemical methods to characterize the cellular responses adjacent to implanted microelectrodes at 1, 3, and 7 days after implantation using single shank planar Michigan-style silicon microelectrode arrays implanted into the cortex of adult male Sprague Dawley rats (225-300g) with N=12 per time point. Electrodes were implanted using stereotactic positioning at +0.2 mm bregma, 3 mm lateral, and 2 mm deep and were anchored with photo-cured adhesive into a polyurethane grommet. As a control, stab wounds were created in the same method, with N=6 at 3 and 7 days. Animals were sacrificed by transcardial perfusion and serial sectioned with a vibrotome. Significant variability existed in the amount of surface hemorrhage and the presence of infracted blood vessels along the implantation tract. Activated macrophages were attached to explanted probes at all postimplantation periods. Activation of perivascular macrophages and extravasation of $ED1^{+}$ cells at the site of injury was evident by 1 day postimplantation. Macrophages were found at the

implant-tissue interface at all time points and were most prevalent at 3 days. At as early as 1 day, $GFAP^+$ astrocytes were absent from the implantation site to about 50 μm, which was maintained at days 3 and 7. There was a significant decrease in neuronal soma within 0-50 μm of the electrode track for stab wound and implanted animals. However for implanted animals, the area of neuronal loss had increased to 0-150 μm at 7 days, suggesting that secondary neuronal cell death is part of the early phase of the foreign body response. Future studies may use pharmacological approaches to understand if these early events can be modulated to improve the long-term functionality of microelectrodes for neuroprosthetic devices.

TABLE OF CONTENTS

LIST OF FIGURES

ACKNOWLEDGEMENTS

Thank you to my advisor, Dr. Patrick Tresco, for his insight and direction and the opportunity to complete this study. Thanks to Brent Winslow for his assistance in the terminal surgeries for all animals in this study. Thanks to Dr. Mike Bridge for developing the ImagePro macros and LabView programs. Thanks to all members of the Keck Center for Tissue Engineering for their advice and support throughout. This work was supported by NIH RO1 NS0467700.

CHAPTER 1

INTRODUCTION

Neuroprosthetic devices

Stimulating and recording electrodes have been developed as research tools and for use in rehabilitative or substitutive neuroprosthetic devices. Examples of neuroprosthetic applications that have achieved clinical success are deep brain stimulators, which are used to alleviate symptoms of Parkinson's disease and other dystonia-related disorders (Benabid, 2001) and cochlear implants, which are used to replace hearing loss in patients with little residual hearing or with deafness (Copeland and Pillsbury, 2004). Recording electrodes are important to the development of a brain-machine or brain-computer interface (BMI or BCI, respectively), which are being developed to restore some degree of motor function or control after degenerative muscle diseases, stroke, and traumatic spinal cord or brain injury (Schwartz, 2006). The realization of a BMI involves a closed-loop system wherein electrical activity in the cerebral cortex can be decoded to accurately predict motor intent and sensory precepts to control an external mechanical device, such as a robotic arm or a cursor on a computer screen (Donoghue, 2002). The proof of principle for developing a BMI has been established in early studies that used macroelectrodes and microwires to record single cortical units (Evarts, 1966; Marg and Adams, 1967; Schmidt et al., 1976; Palmer, 1977). These single-unit recordings

provided evidence that pyramidal neurons in the motor cortex encoded information that strongly correlated to muscle activity (Evarts, 1966, Humphrey, 1970). Further, practical issues of a BMI concerning recording signals from de-efferent cortical regions and peripheral nerve stumps in long-time tetraplegics were eased with studies that illustrated that motor-cortical activation still followed normal somatotopic organization (Shoham et al., 2001) and stimulation of peripheral nerve stumps could generate graded sensory perception in the phantom limb (Dhillon et al., 2002).

Several electrode designs have demonstrated the ability to record cortical activity in rodents, primates, and humans correlating to control of an external device. For example, surface electrodes can record electroencephalograms (EEGs) that detect the massed activity of many neurons, as used in indirect BMIs (Wolpaw et al., 2000). Local field potentials record the activity of populations of synchronized neurons within a microscopic organization, such as a barrel or column, which have similar morphology and function (Markram et al., 2005; Pesaran et al., 2002; Harris et al., 2004; Csicsvari et al., 2003). Invasive recording microelectrodes, including microwires such as the tetrode and microelectromechanical systems (MEMS)-based electrodes and arrays such as the Michigan array and the Utah Electrode Array, are used to record single-units and often target the large pyramidal cell bodies of layer V in the cortex (Evarts, 1966; Humphrey, 1970; Schmidt et al., 1976; Liu et al., 1999; Maynard et al., 1999; Wessberg et al., 2000; Kennedy et al., 2000; Taylor et al., 2002; Serruya et al., 2002; Kipke et al., 2003; Nicolelis et al., 2003; Moxon et al., 2004; Hochberg et al., 2006). Human clinical trials with microelectrodes for recording local field potentials (Csicsvari et al., 2003) and single-units (Kennedy et

al., 2000; Hochberg et al., 2006) illustrate the ability of patients to move a computer cursor to do tasks such as checking email and using spelling programs. These studies are encouraging to the continued development and integration of BMIs for increased communication for "locked-in" or tetraplegic patients.

Recording ability of microelectrodes

MEMS-based microelectrodes, such as silicon electrodes and the cone electrode, have the advantage of a smaller surface area, which minimizes mechanical trauma during implantation, and provide a method for obtaining high-density, high-resolution neuronal recordings (Kennedy et al., 2000; Friehs et al., 2004). To record single-units from adjacent neurons, the recording sites of the microelectrode must be able to discern separable spiking events. To do this, electrodes must be integrated into the surrounding nervous tissue. Mathematical models predict that recording sites must be within 130 μm from active neuronal somas that are most responsible for extracellular activity (Eaton and Henriquez, 2005) to record discernible units, but experimental measurements indicate the maximal distance is closer to 50-100 μm (Henze et al., 2000). The invasive nature of implanted microelectrodes necessitates they be able to record from neurons for chronic time periods, even extending to the life of the patient.

The use of microelectrodes is affected by an inconsistent recording ability for chronic time points, regardless of design or animal model. The recording longevity of an electrode is a measure of the ability to record resolvable neural signals, and the recording longevity of a neural generator is the measure of the ability to track spiking events from the same neuron or group of neurons (Liu et al., 2006). Stability studies have reported that there is an initial stabilization period after implantation, where

recordings may change day-by-day for the first week, and week-by-week for up to 2 months (Liu et al., 1999; Nicolelis et al., 2003; Liu et al., 2006). After the initial stabilization period, studies to date report electrode longevity of 1061 days with microwires in cat cortex (Liu et al., 2006), of 173 days with the Michigan probe in rat cortex (Kipke et al., 2003), of 540 days with the UEA in monkey cortex (Nicolelis et al., 2003), and to a year in a human patient (Hochberg et al., 2006). While these studies indicate that microelectrodes can function at a chronic time point, only about 54-66% of implanted electrodes remained functional after several months postimplantation, and the number of distinguishable single-units greatly degraded over time (Rousche and Normann, 1998; Kipke et al., 2003; Nicolelis et al., 2003; Maynard et al., 2000).

Tissue response at the implant interface

Robust and reliable recording over long time periods requires the electrodes to maintain neural integration with adjacent nervous tissue. It is generally believed that the tissue response to the implanted electrode is a major contributing factor to disintegration at the abiotic-biotic interface. Previous studies have shown that the reaction involves encapsulation by astrocytes, macrophages and microglia (Linell, 1928; Drapiewski et al., 1943; Collias and Manuelidis, 1957; Dymond et al., 1970; Schultz and Willey, 1976; Stensaas and Stensaas, 1976; Stensaas and Stensaas, 1978; Agnew et al., 1986; Turner et al., 1999; Szarowski et al., 2003; Biran et al., 2005), which is also accompanied by up to a 40% decrease in the density of neurons in the recording zone (Edell et al., 1992, Biran et al., 2005).

In general, activated astrocytes, often indicated by swollen cell bodies and hypertrophied processes, form a cellular sheath around the probe by 1 week after implantation (Collias and Manuelidis, 1957; Dymond et al., 1970; Schultz and Willey, 1976; Stensaas and Stensaas, 1976; Stensaas and Stensaas, 1978; Smith et al., 1997; Bramlett and Dietrich, 2002; Rodriguez-Paez et al., 2005; Turner et al., 1999; Szarowski et al., 2003; Biran et al., 2005), which persists but contracts closer to the implant at later time points (Turner et al., 1999; Szarowski et al., 2003). To date, the astroglial scar has been reported to persist at 3 years after implantation (Griffith and Humphrey, 2006), although stab wound experiments show that the initial astrocyte response is transitory, as the electrode track is not found in stab wound animals after several months (Rousche et al., 2001; Csicsvari et al., 2003; Biran et al., 2005). Observed as early as 2 weeks postimplantation, the astroglial scar surrounds a core of activated macrophages and microglia, forming a striated response (Linell, 1928, Collias and Manuelidis, 1957; Turner et al., 1999; Szarowski et al., 2003; Biran et al., 2005).

Glia are intimately integrated in the neuronal signaling network. Astrocytes act as glutamate buffering cells, help to maintain neuronal synapses, and maintain the blood brain barrier (Bezzi and Voltera, 2001). Microglia are the resident macrophages in the CNS, formed by infiltration of prenatal monocytes, and are the primary immune cells in response to brain injury (Becher et al., 2000). In uninjured tissue, ramified microglia continually survey the extracellular environment with dynamic processes and protrusions (Kreutzberg et al., 1996; Stence et al., 2001; Nimmerjahn et al., 2005). In response to injury, microglia and sometimes astrocytes both respond to and

secrete cytokines that may further develop a local inflammatory response (Gareth et al., 1999; Biran et al., 2005).

Early wound healing events in the CNS

Often, the brain tissue response to implanted materials is discussed as two separate events, one that occurs acutely due to mechanical trauma, and a chronic inflammatory response due to the presence of the foreign body. The acute response is largely characterized by the CNS wound healing events in response to the presence of red blood cells, coagulation factors, and complement factors that are induced by the disruption of blood vessels during implantation (Fitch et al., 1999). These events facilitate the activation and migration of macrophages, microglia, and astrocytes that lead to the characteristic glial encapsulation around chronically implanted materials in the CNS (Collias and Manuelidis, 1957; Stensaas and Stensaas, 1978; Szarowski et al., 2003 Turner et al., 1999; Shain et al., 2003).

Injury to the adult brain leads to a complex series of cellular and molecular events, as cells respond to trauma and attempt to repair damaged regions (Fitch et al., 1999; Wieloch and Nikolich, 2006). In general, wound-healing events involve repair of compromised vasculature, removal of debris by white blood cells, reconstructive angiogenesis, and remodeling of affected cell populations and their extracellular matrix. Descriptive studies of the early wound healing response to CNS injury describe similar events (Linell, 1928; Drapiewski, et al., 1943; Collias and Manuelidis, 1957; Szarowski et al., 2003). The early study by Collias and Manuelidis (1957) summarized the tissue reaction to stainless steel electrodes in the cat brain, observed by light microscopy. By day 1 after implantation, they found hemorrhagic

necrosis along the track, infiltration of leukocytes, and activation of macrophages. The macrophage reaction was increased by day 3, though hemorrhage and edema had decreased. At this time, astrocytes became hypertrophied and began to form a boundary around the electrode. Evidence of angiogenesis was also evident by 3 days and continued at 7 days. Day 7 was further characterized by increased numbers of hypertrophied astrocytes, macrophages, the presence of fibroblasts, and demyelinization of neurofilaments. By day 15, new capillaries were found in the necrotic zones, although some edema still persisted. By 30 days, tissue adjacent to the implant showed stages of repair and encapsulation by connective tissue and the astrocyte reaction, which persisted at 60, 120, and 180 days. Thus, the early tissue response, occurring over the first week postimplantation, involves the activation of resident glial populations, neurodegeneration, and repair processes involving connective tissue and neovascularization. The vascular and cellular remodeling events that occur during the first week postimplantation may be responsible for the recording ability of implanted electrodes that has been reported to change day-by-day over the first week (Liu et al., 1999; Nicolelis et al., 2003; Liu et al., 2006). However, it remains unclear when and by what mechanisms the foreign body response eclipses normal wound healing events.

Neurodegeneration involves both the loss of neurons and demyelination of axons, resulting in a loss of functionality of the neural circuit. In response to traumatic brain injury, previous studies found that neuronal cell loss occurred as early as 10 minutes postinjury (Hicks et al., 1996). Both apoptotic and necrotic neurons were found from 1-3 days (Bullock et al., 1991; Dietrich et al., 1994; Crowe et al., 1997; Conti et al.,

1998; Sato et al., 2001) with a secondary, generally apoptotic neuronal loss at 7 days (Liu et al., 1997; Conti et al., 1998; Sato et al., 2001). Delayed neuronal death may be related to increased reactive oxygen species, the glial reaction, and/or neurological deficit, such as axonal target deprivation (Ambrosini et al., 2005). While some studies report no change in the degree of neuronal loss adjacent to implants at more chronic time points (Edell et al., 1992; Biran et al., 2005), others show a progressive neurodegernative process that may occur up to 1 year following traumatic brain injury (Smith et al., 1997; Bramlett and Dietrich, 2002; Rodriguez-Paez et al., 2005). Overall, active cell death as well as passive necrosis may be responsible for neuronal cell death in response to CNS injury, and likely there is not a single cause of neurodegeneration (Crowe et al., 1997; Martin et al., 1998; Heidenreich, 2003). In addition to determining the mechanism of neuronal cell death, it is important to understand the degree of loss due to the initial injury and to the presence of the indwelling electrode. Intervention strategies may be used shift the degree of neuronal loss due to the foreign body response towards the stab wound phenotype.

Many of the studies in this field have focused on the long-term or chronic tissue response with less attention to the events that precede glial encapsulation. The focus of the present study was to examine the earliest events that follow the implantation of Michigan-style planar silicon microelectrode recording arrays in rat cortex. To do this, we used immunohistochemical methods to characterize the cellular responses adjacent to indwelling microelectrodes and stab wound tracks to differentiate the foreign body response at 1, 3 and 7 days postimplantation. In general, we found that the tissue response to implanted Michigan-style microelectrode arrays in the earliest

events is largely characterized by the foreign body response, where the macrophage response in implanted animals was increased due to the presence of the indwelling electrode, which contributed to the astrocyte loss and decrease in neuronal density immediately surrounding the electrode. Surface hemorrhage and the presence of micro-hemorrhages and disrupted blood vessels along the implantation tract were observed at days 1 and 3. In the least reactive cases, ED1 labeled macrophages were present both attached to retrieved electrodes and in the tissue immediately adjacent to the implant site at 1 day in both stab wound and experimental animals, with a maximal response at 3 days. At as early as 1 day, GFAP labeled astrocytes were absent from the implantation site and in the surrounding parenchyma to varying degrees, which was maintained at days 3 and 7. This response suggests that astrocytes are sensitive to early events in the foreign body response, as stab wound animals showed little or no loss of astrocytes at the electrode-tissue interface. Further, the zone of neuronal loss was increased at day 7, suggesting that secondary neuronal cell death is also part of the early phase of the foreign body response.

CHAPTER 2

MATERIALS AND METHODS

Microelectrodes and grommets

Single shank, planar, 16 recording site silicon microelectrode arrays were fabricated and supplied by the Center for Neural Communication Technology (CNCT) at the University of Michigan. All electrodes had the following dimensions within the cortex: length, 2 mm; width, from 75 μm tapering to 2 μm at the tip; and thickness, 15 μm along the shank and 2 μm at the tip. All electrodes were cleaned by soaking in 70% ethanol for 30 seconds followed by sterile DI H_20 for 30 minutes. Electrodes were gas sterilized with EtO^-. Polyurethane grommets, which are access ports that snap into the burr hole drilled in the skull, were fabricated as described (Young, et al. 2003). Prior to implantation, grommets were soaked in 70% ethanol for 30 seconds followed by sterile DI H_20 for 30 minutes. After cleaning, grommets were inspected for swelling and correct hardness.

Animal surgery

All procedures involving animals were conducted using sterile technique in accordance with protocols approved by the University of Utah Institutional Animal Care and Use Committee. Implantation and terminal surgery methods are similar to those previously described (Biran et al., 2005). Adult male Sprague Dawley rats

(225-300g) were weighed and anesthetized with a cocktail of ketamine (65 mg/kg), xylazine (7.5 mg/kg), and acepromazine (0.5 mg/kg). Fully anesthetized animals were prepared for surgery by covering the eyes with ophthalmic ointment and shaving the head. The scalp was disinfected with isopropanol followed by butadiene. Animals were transferred to a stereotaxic frame (Stoelting Co., Wood Dale, IL) set under a stereomicroscope. A midline incision extending to the length of the skull was made. For all implant types, a 3 mm diameter burr hole was created through the depth of the skull with a custom fabricated trephinated drill bit under stereotactic control and copious irrigation with sterile phosphate buffered saline (PBS). The center of the hole was positioned at coordinates +0.2 forward and 3 mm lateral to bregma. The cortical bone plug was removed with fine forceps under stereomagnification. The dura was carefully opened with a 21G needle and bleeding was controlled with cotton tip applicators. A custom-made polyurethane grommet was fastened to the skull by design. Microelectrodes were lowered 2 mm into the brain under stereotactic control, with the flat side containing recording sites oriented forward along the coronal plane. The electrodes were anchored in the grommet by photocurable adhesive. The scalp incision was closed with 5/0 silk sutures. A schematic of the implant in rat cortex is shown in Figure 1.

As a control, stab wounds were created with the same type of microelectrode for adult male Sprague Dawley rats (225-300g). After opening the dura and fastening the grommet to the skull, microelectrodes were lowered into the brain to the same depth and in the same manner as described above. The microelectrode was withdrawn after 2 minutes, the grommet sealed with photocurable adhesive, and the scalp closed.

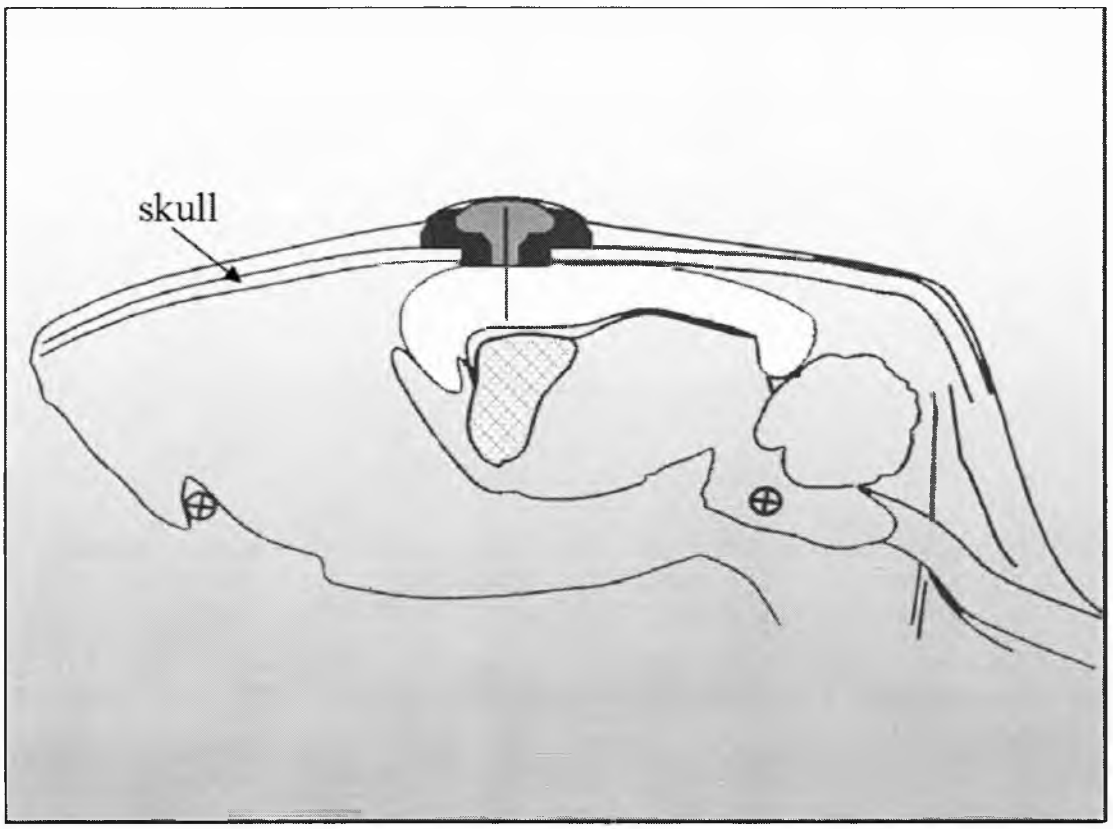

Figure 1. Schematic of implant in rat cortex. Electrodes were implanted at the border of motor and sensory cortices of front fore limb at 0.2 mm forward of bregma, 3.0 mm lateral of the midline, and lowered to a depth of 2.0 mm, with recording sites facing forward. A custom grommet (black) was fit into the skull by design, and an electrode (black line) was lowered through the grommet and into the cortex (white) using a manipulator. The electrode was fixed in place by photo curable adhesive (dark gray). Cortex is white, striatum is hatched, grommet is black, and photocurable adhesive is dark gray. Scale bar= 2mm.

At 1, 3, or 7 days after implantation, N=12 per time point, and 3 or 7 days after stab wound, N=6 per time point, animals were again weighed and then terminally anesthetized with a mixture of ketamine (70 mg/kg) and xylazine (30 mg/kg). Animals were perfused transcardially at a flow rate of 50 mL/min with 250 mL of ice-cold PBS, followed by 250 mL of fresh ice-cold 4% (w/v) paraformaldehyde. The brains were removed and grommets were carefully unfastened from the skull and lifted upwards to remove electrodes from the cortex of implanted animals. Brains and implants were postfixed overnight in 4% paraformaldehyde and later stored in PBS with 0.1% NaN_3.

Sectioning and immunostaining

Following postfixation, animal brains were sectioned horizontally (N=8 per time point, implanted animals or N=6 per time point, stab wound) or coronally (N=4 per time point, implanted animals) to a thickness of 40 μm on a vibratome (Vibratome, Inc., St. Lous, MO) and serially collected. Horizontal sections were collected perpendicular to the electrode or stab wound track, beginning at the surface of the cortex to a depth of approximately 3mm, well below the area of implantation. Coronal sections were cut parallel to the implant track. Sections were stored as free-floating sections one per well in culture plates filled with 1xPBS containing 0.1% NaN_3 until processed for immunostaining. Electrodes were removed from the base of the grommets with microdissection scissors and similarly prepared for immunostaining.

Approximately one section for every consecutive 160 μm within the cortex, for a total of 11 sections per animal, was stained with each antigen combination. Primary

antibodies were used to specifically identify astrocytes, activated macrophages, and neuronal nuclei. Astrocytes were identified by the use of polyclonal rabbit IgG anti-glial fibrillary acidic protein (GFAP) (DAKO, Carpinteria, CA), which is a marker for the intermediate filament protein. Monoclonal IgG1 anti-CD68 (ED-1) (Serotec, Raleigh, NC) was used to label a lysosomal glycoprotein expressed by activated macrophages. Resident macrophages, termed microglia, are indistinguishable from blood-borne macrophages with this marker. Monoclonal IgG1 anti-NeuN (Chemicon, Temecula, CA) identified neuronal nuclei by labeling a DNA-binding protein. Secondary antibodies were isotype-matched Alexa-488 and Alexa-594 antibodies (Molecular Probes, Carlsbad, CA). Each section was stained for GFAP and costained for either ED-1 or NeuN. Primary (1/1000 dilution) and secondary (1/500 dilution) antibodies were diluted in a blocking solution consisting of 4% (v/v) goat serum, 0.5% (v/v) Triton-X-100, and 0.1% (w/v) sodium azide in 1xPBS, pH 7.4. Sections were incubated with blocking solution for 1 hour at room temperature before applying primary antibodies overnight at 4°C. After three PBS rinses, secondary antibodies containing 1.0 μM 4',6-diamidino-2-phenylindole (DAPI) (Molecular Probes) to identify all cell nuclei were added to the appropriate tissue sections for 2 hours at room temperature. After washing with PBS, sections were mounted onto microscope slides using Fluoromount-G (Southern Biotech, Birmingham, AL) and covered with a No.1 cover glass. Retrieved electrodes were immunostained by applying block solution in the same manner. Primary antibodies (1/500 dilution) for GFAP and ED-1 and corresponding secondary antibodies (1/220 dilution), counterstained with DAPI were applied as described above. Electrodes retrieved from

stab wound animals were stained with 1% (v/v) eosin solution in EtOH for 2 minutes to visualize any protein attached to the electrodes. All implanted animals were batch stained to minimize variability in staining intensities, allowing for a way to differentiate relative staining intensities over time. Stab wound animals and electrodes were also batch stained.

Imaging and quantification

Digital images were acquired with a Coolsnap color CCD digital camera (Roper Scientific, Trenton, NJ) attached to a Nikon E600 upright microscope (Nikon, Melville, NY) using Image Pro 4.0 software (Media Cybernetics, Silver Spring, MD). Digital images were collected in RGB color at 12 bits per channel with a spatial resolution of 1392 x 1040 pixels. Exposure times were chosen at subsaturating levels and were used consistently with respect to each marker. Light field correction images, no-primary control images, and dark field images were taken to correct for a nonhomogenous illumination field, and changes in background staining and ambient light, respectively. Images were captured with the implant site in the center and were oriented to be consistent with anatomical maps and to locate the side of the electrode containing the iridium recording sites. To acquire depth information, images were ordered with respect to proximity to the corpus callosum.

To quantify the tissue response adjacent to the implant or stab wound track, pixel intensity data were analyzed with respect to distance from the tracks. The method used to generate profiles of pixel intensity with custom LabVIEW programs (National Instruments Co., Austin, TX) is described in (Young et al., 2003). Digital 10x images were converted to 8 bit per channel and the red, green, and blue channels

were merged for each tissue section using custom Image Pro macros. Light field corrections were applied to merged images. Merged images were then transferred into a LabVIEW program that created linear profiles perpendicular to the long orientation of the implant. Equally spaced lines were drawn with a constant density and spacing between 2.5 and 2.75 μm, depending on track size (Figure 2). For implanted animals, the electrode track was identified using DAPI and ED-1 markers to define the location and width of the track. ED-1 and GFAP were useful in determining the location of the stab wound. Line profile data were averaged to create one profile for each color channel. The location of the implant or stab wound track was determined for each profile; in this way, the average profile for each animal was calculated with respect to distance from the electrode track. Profiles were adjusted for ambient light and background staining determined by no-primary control images.

Average line profile data for each animal were transferred to Microsoft Excel. Graphs were generated to represent average antigen intensity profiles for each time point. Profiles were normalized to the maximum intensity value for implanted and for stab wound animals. Further, the maximum intensity values and their positions with respect to the implant track for GFAP and ED-1 profiles were determined and compared for all implanted animals. Data presented as mean values ±SEM.

The degree of neuronal loss was measured by counting the number of $NeuN^+$ nuclei by overlaying each image with a 50 x 100 μm mesh (Figure 3). The grid was adjusted so that the electrode track was bisected through the long axis, similar to the position of the line profiles shown in Figure 2. Neuronal bodies were counted as a function of distance from the track in 50 μm increments; to a distance of 500 μm.

Figure 2. Example of the line profile program created in LabVIEW. A) Equally spaced line profiles, between 2.55 and 2.75 μm, are drawn across long axis of the electrode or stab wound track, which is in the middle of the image (dashed horizontal line). The endpoints of the track are determined with DAPI and ED-1 staining. B) Panels on the left of the figure show the pixel intensity as a function of distance for each of the color channels: red, green, and blue. The average of all the line profiles for a given image are shown in C, separated by color channel. The processed profile line intensity graph is exported to another LabVIEW program that averages all the profile data per animal.

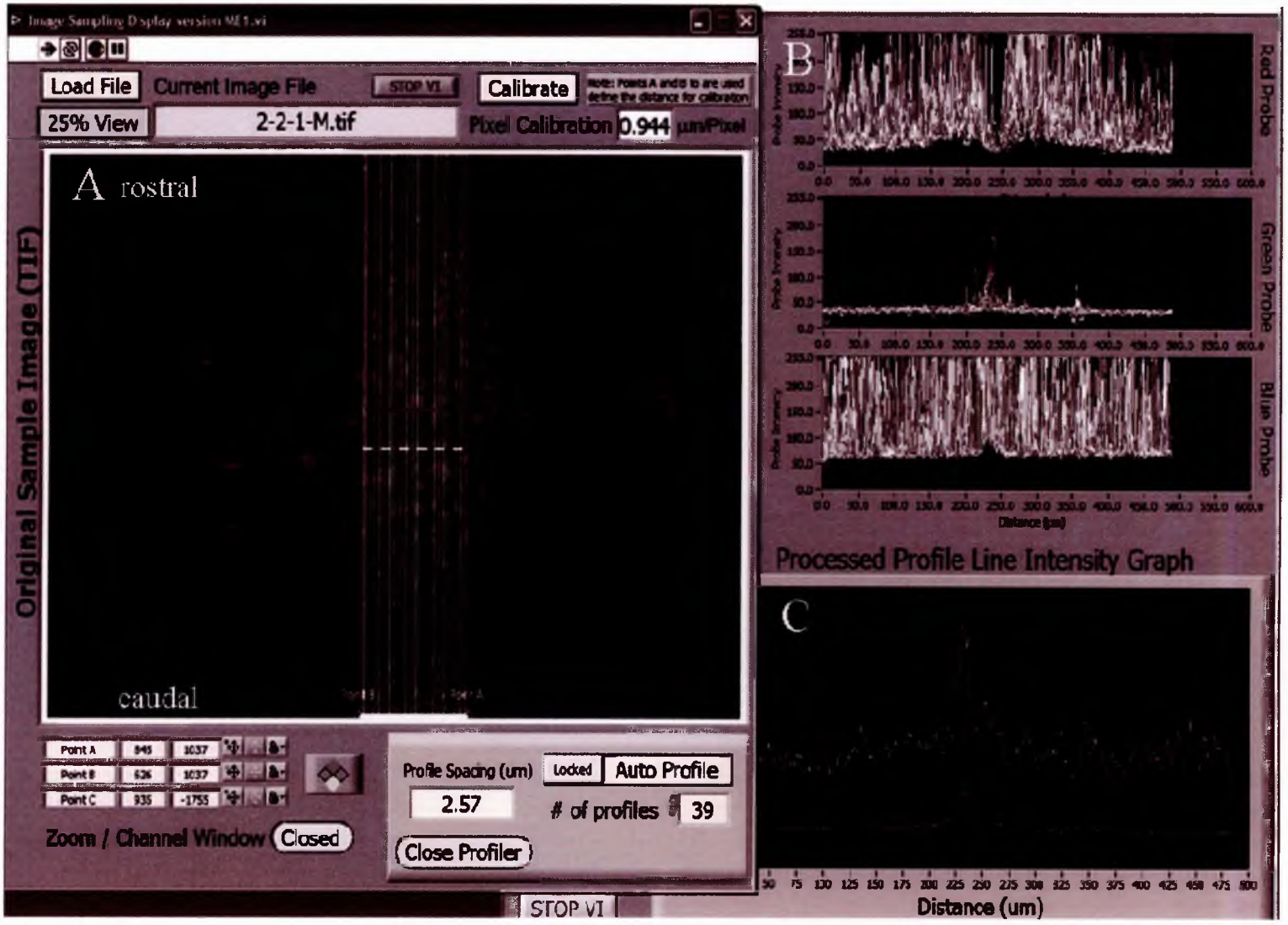
Load File
Current Image File
STOP VI
Calibrate
25% View
2-2-1-M.tif
Pixel Calibration 0.944 µm/Pixel
A rostral
caudal
Original Sample Image (TIF)
Point A 845 1037
Point B 626 1037
Point C 935 -1755
Zoom / Channel Window Closed
Profile Spacing (um)
Locked
Auto Profile
2.57
# of profiles 39
Close Profiler
STOP VI
B
Red Probe
Green Probe
Blue Probe
Distance (um)
Processed Profile Line Intensity Graph
C
Distance (um)

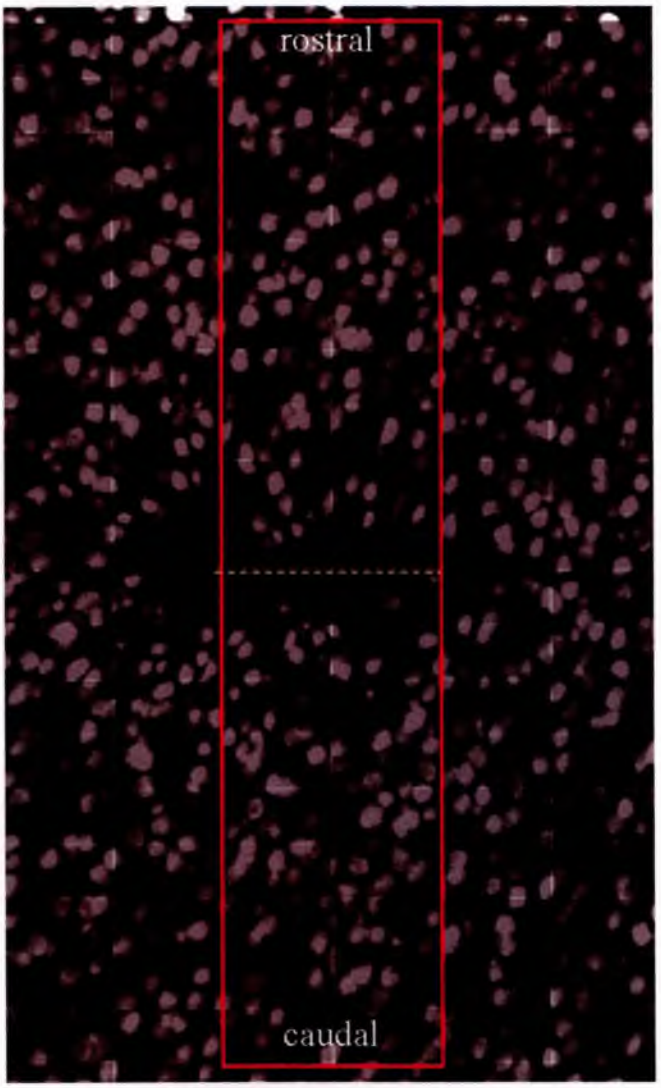

Figure 3. Quantification of neuronal density. For each image, a 50 x 50 μm grid was overlaid so that the electrode or stab wound, seen as a dashed line in this figure, track was bisected through the long axis. For implant tracks that showed a loss of tissue, seen as a hole, the grid was placed on the edge of the hole. Neuronal bodies were counted as a function of distance in 50 μm increments to a distance of 500 μm, region of interest is boxed.

Bins at comparable distances both above and below the electrode track were averaged. Counts were ordered with respect to depth in the cortex and analyzed as a percentage of the average number of neurons 450-500 μm from the electrode track. The number of neuronal cell bodies at this distance was assumed to be representative of uninjured tissue. Neuronal counts for a depth of 1 to 2 mm in the cortex were included in the analysis, as many sections were damaged within the first 1 mm due to surface bleeding and necrosis.

Statistical analysis

To analyze the distribution of glial activity over time, one-way ANOVAs, $p \leq 0.05$, were used. A one-way ANOVA was used to compare both the value and the distance of the maximum intensity value for each time point. A one-way ANOVA was also used to compare NeuN counts for implanted and stab wound animals with respect to distance. Significance between groups was determined with a t-test, assuming unequal variances with $p \leq 0.05$ where appropriate. Also, the number of neuronal bodies proximal to the electrode track was compared to those 450-500 μm away individually for each time point.

CHAPTER 3

RESULTS

All animals recovered from surgery with no evidence of infection and survived the duration of the experiment. There was no noticeable behavioral difference for any experimental animals. This observation was further supported by weight gained in animals sacrificed at 3 and 7 days postsurgery; animals sacrificed after one day either did not have a significant weight loss. There was no difference in weight gain or loss between implanted and stab wound animals (Figure 4).

Gross anatomy of fixed, perfused brains

Epidural blood clots were found below the scalp, enclosed in connective tissue, for most animals sacrificed at 1 and 3 days. The upper surface of explanted brains showed evidence of bleeding and swelling at the implant site. The contralateral hemisphere was representative of normal, uninjured tissue. Surface reactivity was maximal at 1 day, and diminished over time. Four of the explanted brains at 7 days showed no evidence of blood at the implant site. Examples of the most reactive hemorrhagic and average responses with respect to time are found in Figure 5. Hemorrhages at the surface of the brain at the implant site were also correlated to increased tissue reactivity in the more superificial cortical layers. These early

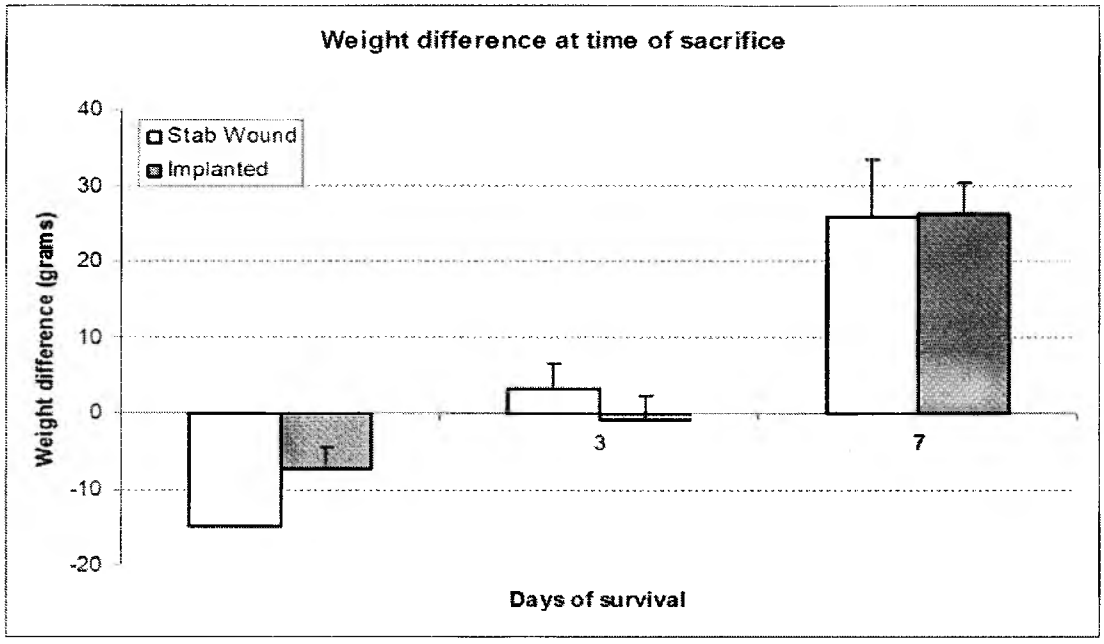

Figure 4. Chart of the weight difference for stab wound and implanted animals between time of initial surgery and time of sacrifice. Animals sacrificed 24 hours after surgery generally lost a small amount of weight. By 7 days, animals had gained weight, one indication of normal behavior postsurgery. There was no difference between weight measures for stab wound and implanted animals, 1-way ANOVA $p < 0.05$. Error bars are SEM. There is only one stab wound animal sacrificed at 1 day.

bleeding and necrotic events have previously been described for implanted macroelectrodes (Linell, 1928; Drapiewski et al., 1943; Collias and Manuelidis, 1957), but have not been described in response to implanted planar microelectrodes such as the Michigan electrode. Further, the contralateral hemispheres for all animals, including the most reactive, showed no staining for ED-1, normal distributions of nonhypertrophied $GFAP^+$ astrocytes, and normal distributions of neuronal markers.

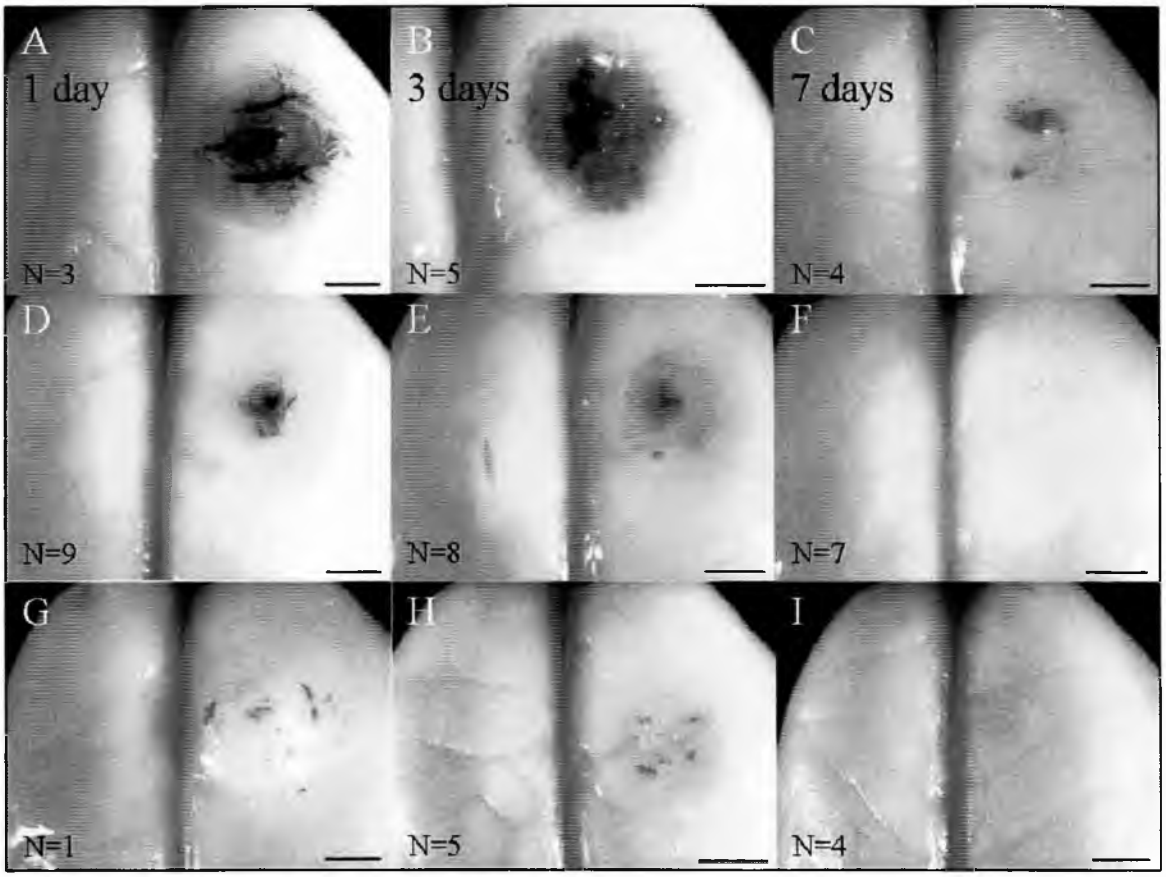

Figure 5. Gross anatomy of the upper surface of perfused, explanted brains. Animals sacrificed at 1 (left panel), 3 (middle panel), and 7 days (right panel), showing the implant site and the contralateral, uninjured cortical hemisphere. The top row of images (A-C) are examples of the most reactive hemorrhagic response for each time point. N= number of animal of each type of case. The middle row (D-F) are the average responses for implanted animals. (G-I) shows the average responses for stab wound animals. There was only one stab wound animal sacrificed at 1 day. Blood clots were often observed on top of the implant site for implanted and stab wound animals sacrificed at 1 and 3 days. Scale bar = 2.5 mm.

Vasculature disrupted during implantation

During implantation, bladelike electrodes rupture vasculature, especially capillaries, along the implantation track. Hemosiderin is a breakdown product of hemoglobin released red blood cells upon phagocytosis by activated macrophages; the breakdown of red blood cells contributes to a cytotoxic respiratory burst. Hemosiderin deposits were found in the electrode tracks in both implanted and stab wound animals sacrificed at 1 and 3 days, an example at 3 days is shown in Figure 6. Hemosiderin deposits were not typically observed at the electrode track for animals sacrificed at 7 days. Adjacent vasculature was also affected in 1 and 3 day animals: vessels contained hemosiderin deposits, and infarcted tissue was observed at remote distances from the implant site. Often, in infarcted areas where NeuN and NF remained, $GFAP^+$ astrocytes were absent, and fragmented GFAP was observed.

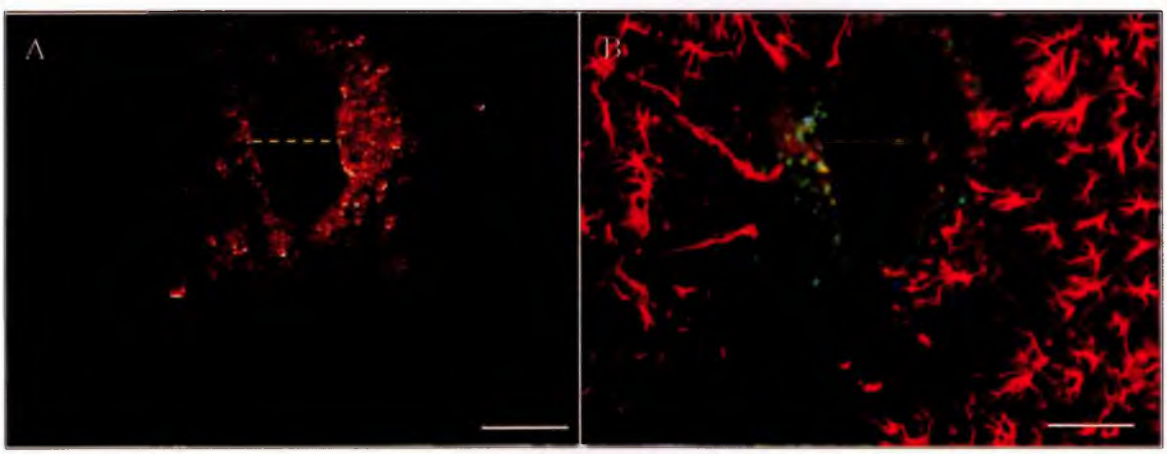

Figure 6. Example of hemosiderin deposit at the electrode track at 3 days postimplantation. A) Lightfield image of hemosiderin deposits surrounding electrode track. B) Fluorescent image of same section in (A) of GFAP (red), ED-1 (green), and DAPI (blue). ED-1+ macrophages are present immediately adjacent to the electrode track. GFAP+ astrocytes are absent around the track. The implant track is shown as a hole. Electrode footprint is dotted line. Scale bar = 100 μm.

Cellular attachment to explanted electrodes

Upon removal from fixed, perfused brains, electrodes and grommets were largely clear of connective tissue. Grommets were easily removed from the skull and all electrodes remained fixed within the adhesive. Under fluorescence, DAPI was observed on all explanted electrodes at all time points. Most of the cells attached to indwelling electrodes were colocalized with the ED-1 antigen but not for GFAP (Figure 7). Visualization with scanning electron microscopy (SEM) showed that wellspread cellular material attached to the surface of the electrode corresponded to cell clusters visualized by immunostaining. This indicates cellular adhesion and spreading of activated macrophages on the surface of the electrode, which may be a factor in the increased and persistent tissue response due to the presence of a foreign body. Small anuclear cells, that appeared to be red blood cells, were also found attached to electrodes using SEM at 7 days postimplantation. Electrodes removed from stab wound animals were covered with protein along the entire shank, determined by Eosin staining (data not shown). Further, cell nuclei identified by DAPI were observed sparsely attached to explanted stab wound probes. Colocalization with ED-1 and GFAP were not conclusive in identifying cell types on stab wound electrodes due to high background staining.

Activated macrophages are present at the electrode-tissue interface

Consistent with previous work (Linell, 1928; Drapiewski et al., 1943; Collias and Manuelidis, 1957; Szarowski et al., 2003), activated macrophages, determined by the expression of ED-1, were observed around the electrode track by 1 day postinjury.

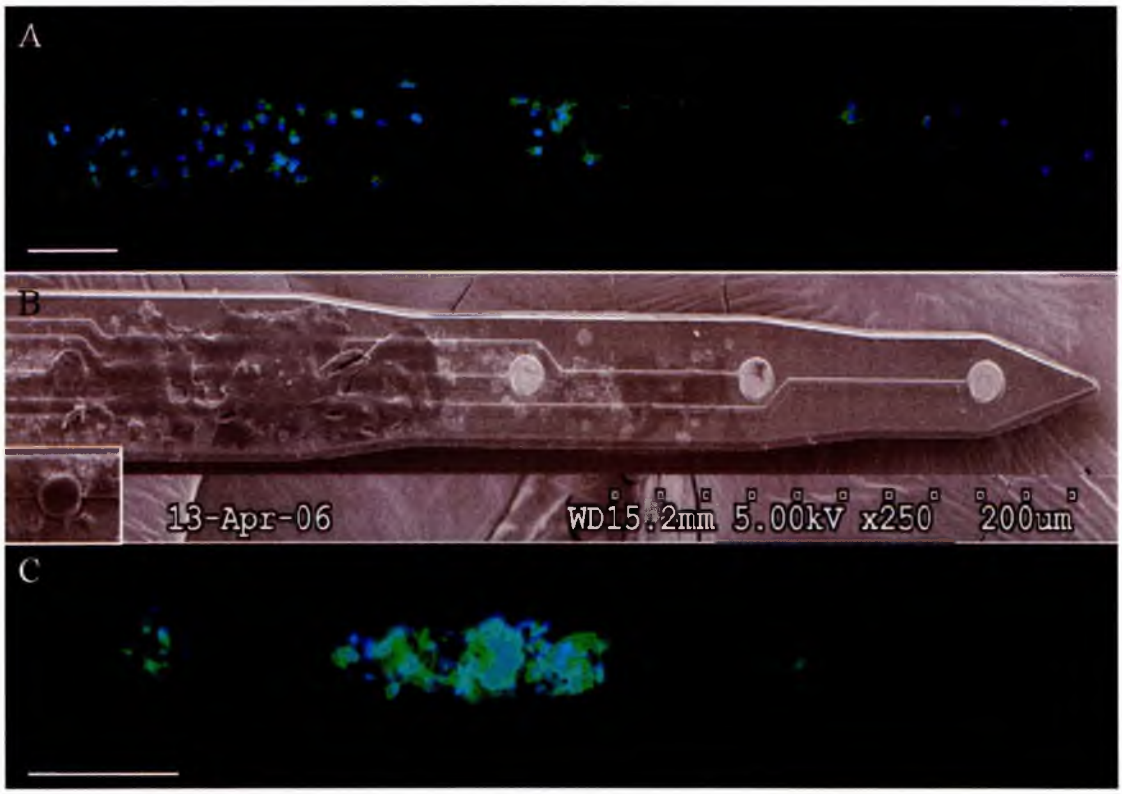

Figure 7. Cellular attachment to explanted electrodes. A) Representative fluorescence illumination of an explanted electrode from an animal sacrificed at 1 day. DAPI (blue) is colocalized with ED-1 (green) almost exclusively. Activated macrophages attached to electrodes as early as 1 day postimplantation. B) SEM visualization of an electrode explanted at 7 days. Cellular material is seen attached and wellspread on the electrode surface. Box shows the presence of red blood cells attached to electrode. C) Fluorescent image of the same probe in (B), for DAPI (blue) and ED-1 (green). Most of cellular material is positively stained for activated macrophages. Scale bar = 100 μm.

Upregulation of perivascular macrophages and presumptive extravasation of monocytes from the vasculature towards the implant site was observed at 1 and 3 days, seen in Figure 8 at 3 days. At 1 day, macrophages surrounded the implant track with a radius of 60 μm. ED-1 reactivity was most broadly distributed in tissue adjacent to the implant track at 3 days, with an average radius of about 75 μm. By 7 days, the macrophage response had reached its peak intensity and had contracted around the electrode track, to a radius of about 40 μm. The average peak intensity value and position for implanted animals at each time point illustrate the evolution of the macrophage response from a distance of 6 μm at 1 day, to 13 μm at 3 days, and 3 μm from the implant site by 7 days (Figure 9). The distances were found to be significantly different among all time points, ANOVA $p<0.05$. The peak intensity value was different between 1 and 3 days, but did not significantly change at 7 days, t-test with unequal variance $p<0.05$.

ED-1 labeled macrophages were also observed at the wound site for stab wound animals at 3 and 7 days. The radius of the macrophage reaction at 3 days postinjury was 45 μm, which decreased to about 20 μm by day 7. Although direct comparisons of line profile data cannot be made between stab wound and implanted animals since they were not batched stained, both the intensity and the breadth of the macrophage reaction appeared increased in implanted animals compared to stab wound animals.

Astrocyte loss is an early event in the foreign body response

While astrogliosis is a hallmark of the chronic inflammatory response surrounding implanted microelectrodes, the presence of $GFAP^+$ astrocytes was markedly decreased adjacent to the electrode track in implanted animals at the early

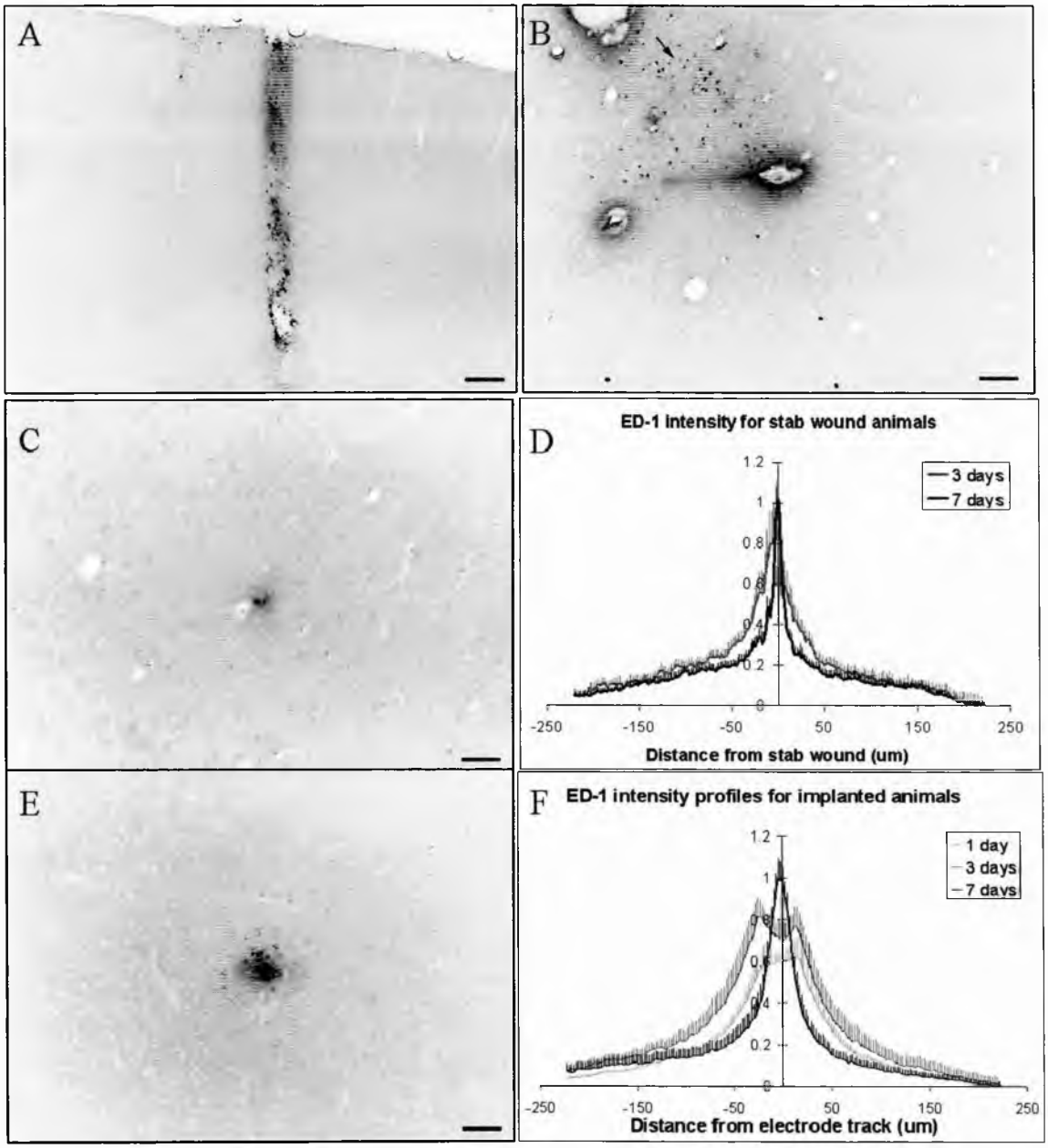

Figure 8. Activated macrophages respond quickly to injury. A) Representative coronal image at 3 days showing ED-1 reactivity along the length of the electrode track through the cortex. B) Horizontal image of ED-1+ cells at the site of injury at 3 days postimplantation. Macrophages activated in surrounding tissue; presumptive migration of macrophages towards implant site indicated by arrow. C) Representative horizontal ED-1 image for stab wound animals. D) Average intensity profiles of ED-1 as a function of distance from the electrode track for stab wound animals at 3 and 7 days. E) Representative horizontal ED-1 image for implanted animals. F) Average intensity profiles of ED-1 for implanted animals at 1, 3, and 7 days. ED-1 labeled macrophages appear to be increased in implanted animals compared to stab wounds at each time point. Error bars are SEM. Scale bar = 100 μm.

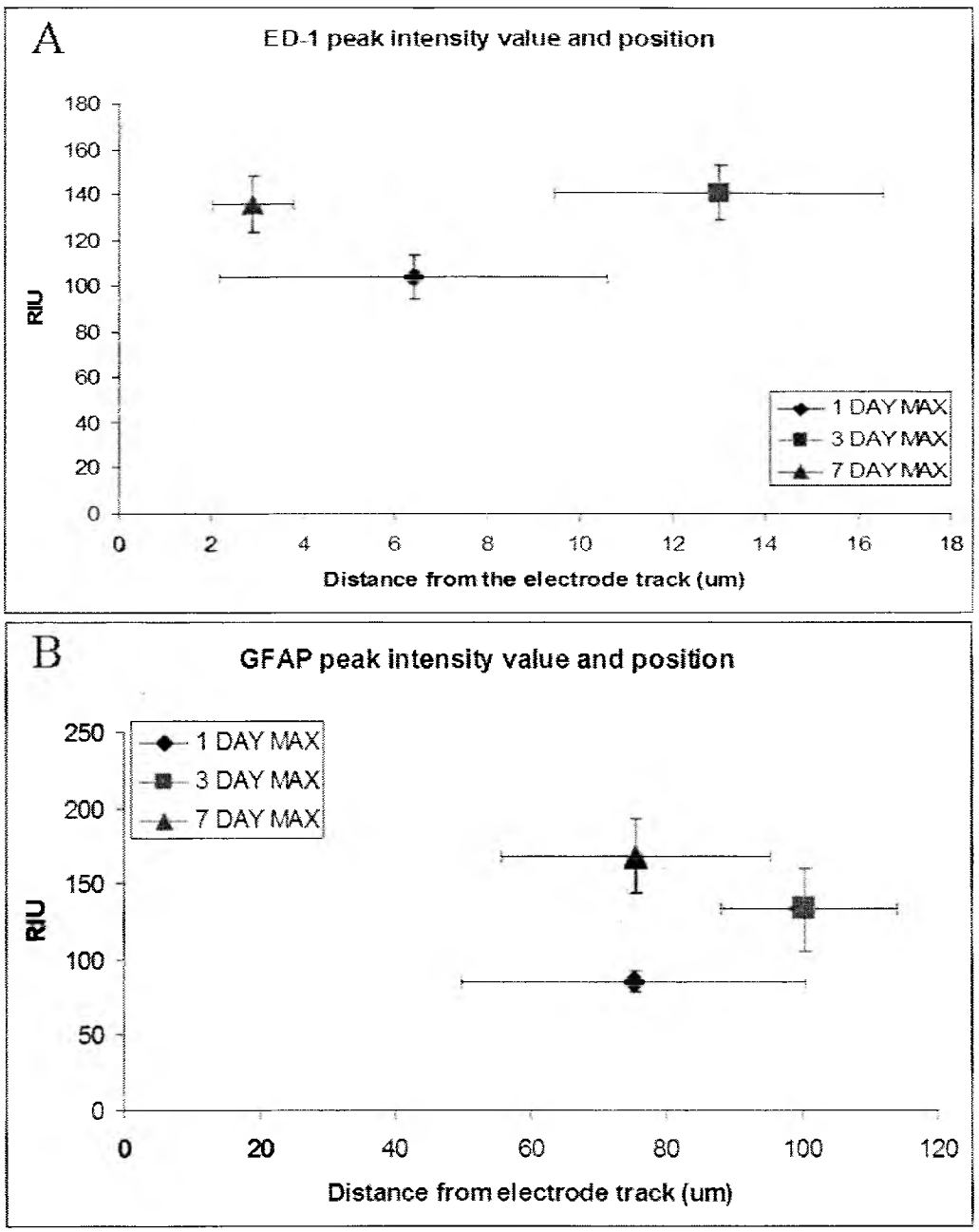

Figure 9. Average peak intensity values and position for ED-1 and GFAP antigens. A) The average peak intensity value and position from the electrode track for ED-1 was located for implanted animals as a function of time. The distance of the peak intensity was different among all time points, increasing from 1 day to 3 days, and contracting at 7 days. The peak intensity value increased from 1 day to 3 days, but did significantly change by 7 days. B) Average peak intensity value and position from the electrode track for GFAP as a function of time. The peak value of GFAP was located outside the zone of astrocyte loss, which did not change over time. The intensity value increased over time, as astrocytes became increasingly hypertrophied. Statistical analysis done with a 1-way ANOVA, $p<0.05$. Error bars are ±SEM.

time points (Figures 10 and 11). Astrocytes were absent for the first 40 μm around the implant track at 1 day, and the position of the front of astrocytes was not significantly different at 3 or 7 days. Outside the zone of astrocyte loss, remaining astrocytes had upregulated expression of GFAP. The average peak intensity value and position of GFAP was plotted for implanted animals at each time point (Figure 9). While the distance of the maximal GFAP reactivity did not change over time from about 80 μm, the intensity value increased over time, ANOVA $p<0.05$. This is reflective of an astrocyte reaction that was progressively hypertrophic with evidence of hyperplasia adjacent to the electrode track by 7 days. See Figure 11. In addition, astrocytes within the surrounding 500 μm were increasingly hypertrophic over time.

In contrast to the astrocyte loss surrounding the electrode track in implanted animals, stab wound animals showed no loss of adjacent $GFAP^+$ astrocytes. In fact, hypertrophic astrocytes were present at the wound site and to a distance of about 100 μm from the wound, often demarcating the location of the wound. The difference between the astrocyte response in implanted and stab wound animals represents the change due to the presence of a foreign body in the CNS (Figure 10).

Neuronal cell loss, early and secondary events

The density of neuronal cell bodies was decreased within the first 50 μm from the implant site for all implanted and stab wound animals (Figure 12). In animals with indwelling implants, the average degree of neuronal loss within the first 0-50 μm was 70% from background measures (400-450 μm from the implant site). Within the first 0-100 μm, neuronal density was decreased by about 50%, which is comparable to

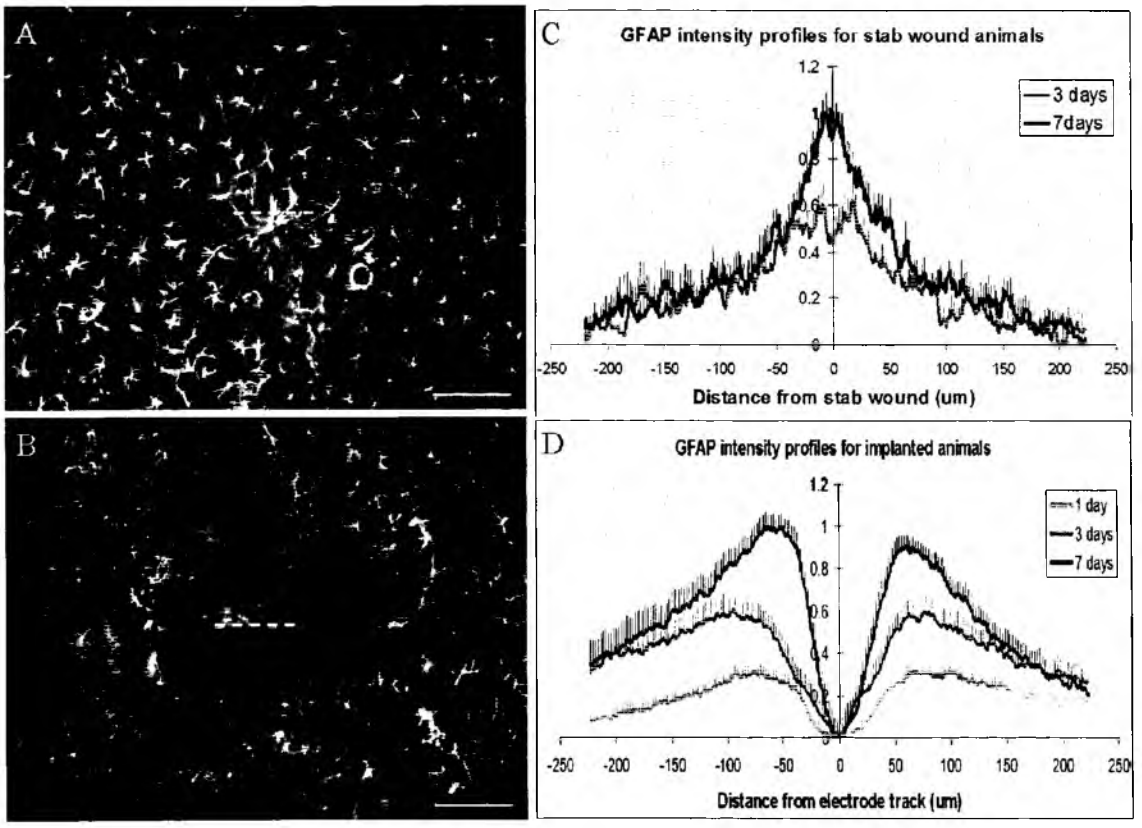

Figure 10. Astrocyte loss is an early event in the foreign body response. A) Representative horizontal stab wound image at 3 days. GFAP staining shows that hypertrophied astrocytes are present at the wound site, dotted line, with no loss of astrocytes around the stab wound track. B) Representative horizontal image of GFAP reactivity around the electrode track, dotted line, in the least reactive case. GFAP+ astrocytes are absent in immediately surrounding parenchymal to varying degrees. This zone of astrocyte loss was maintained at all time points. Scale bar = 100 μm. C and D) Distribution of the relative intensity of GFAP as a function of distance from the stab wound or electrode track. C) Average intensity profiles for stab wound animals at 3 and 7 days. GFAP is found at the wound site, with no evidence of astrocyte loss. Astrocytes are hypertrophied at a radius of about 100 μm from the wound site. D) Average intensity profiles for implanted animals at 1, 3, and 7 days. The loss of GFAP is reflected in the bimodal antigen distribution. Astrocytes continually upregulate GFAP adjacent to the electrode track. Error bars are SEM.

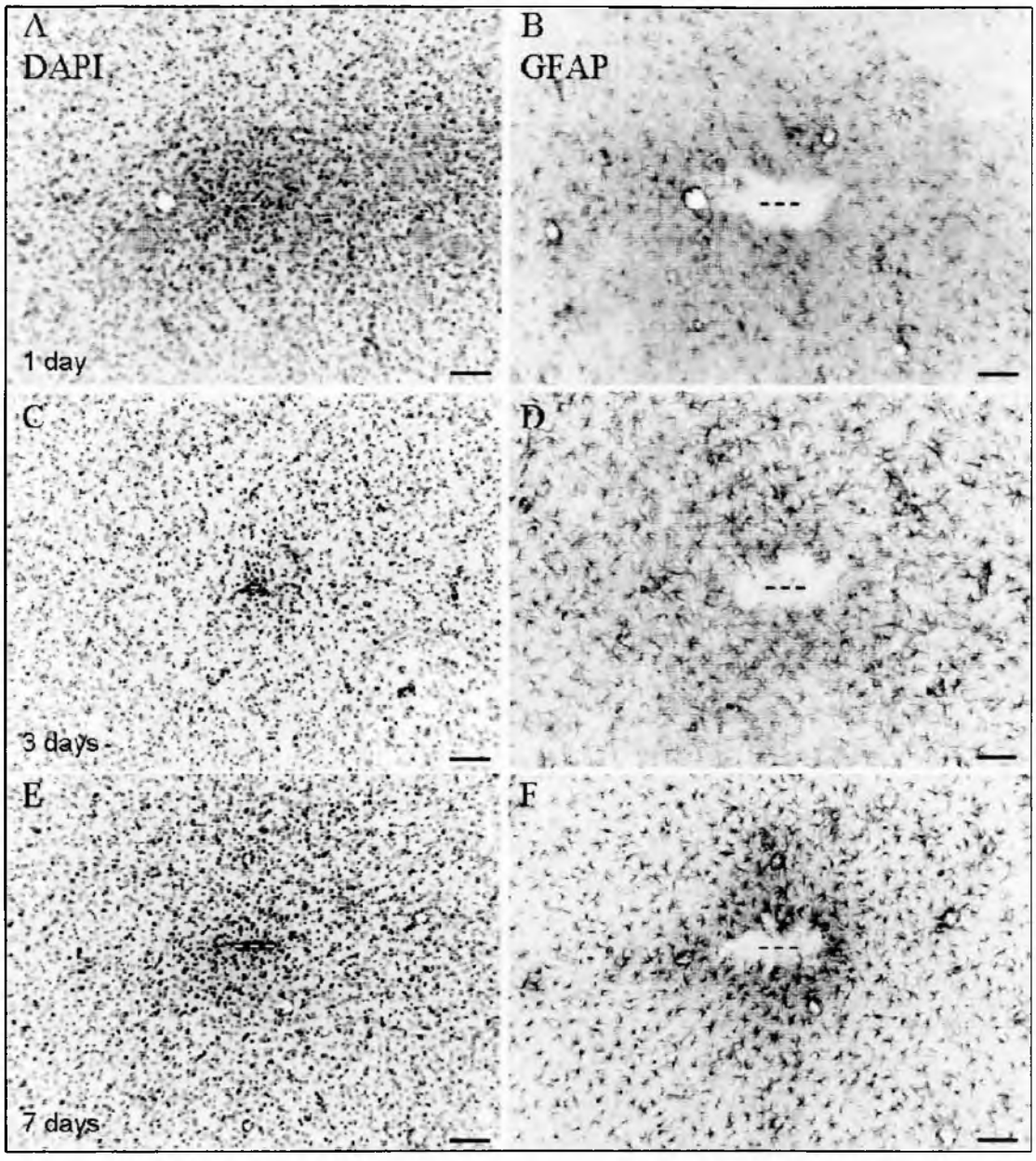

Figure 11. Representative horizontal images of GFAP response in implanted animals as a function of time. Images for sections stained for both DAPI (A, C, E) and GFAP (B, D, F) at 1 day (A, B), 3 days (C, D), and 7 days (E, F). Images for DAPI illustrate presence of cell nuclei even within the zone of astrocyte loss. A and B) At 1 day postimplantation, astrocytes were absent in tissue surrounding electrode track. Some remaining astrocytes became hypertrophied. C and D) By 3 days, astrocytes at the zone of loss and within surrounding 500 μm had upregulated GFAP. E and F) Hypertrophied astrocytes began to form a cellular sheath by 7 days. There was also increased cellularity at the implant site, seen in E. Dashed lines denote implant site. Scale bar = 100 μm.

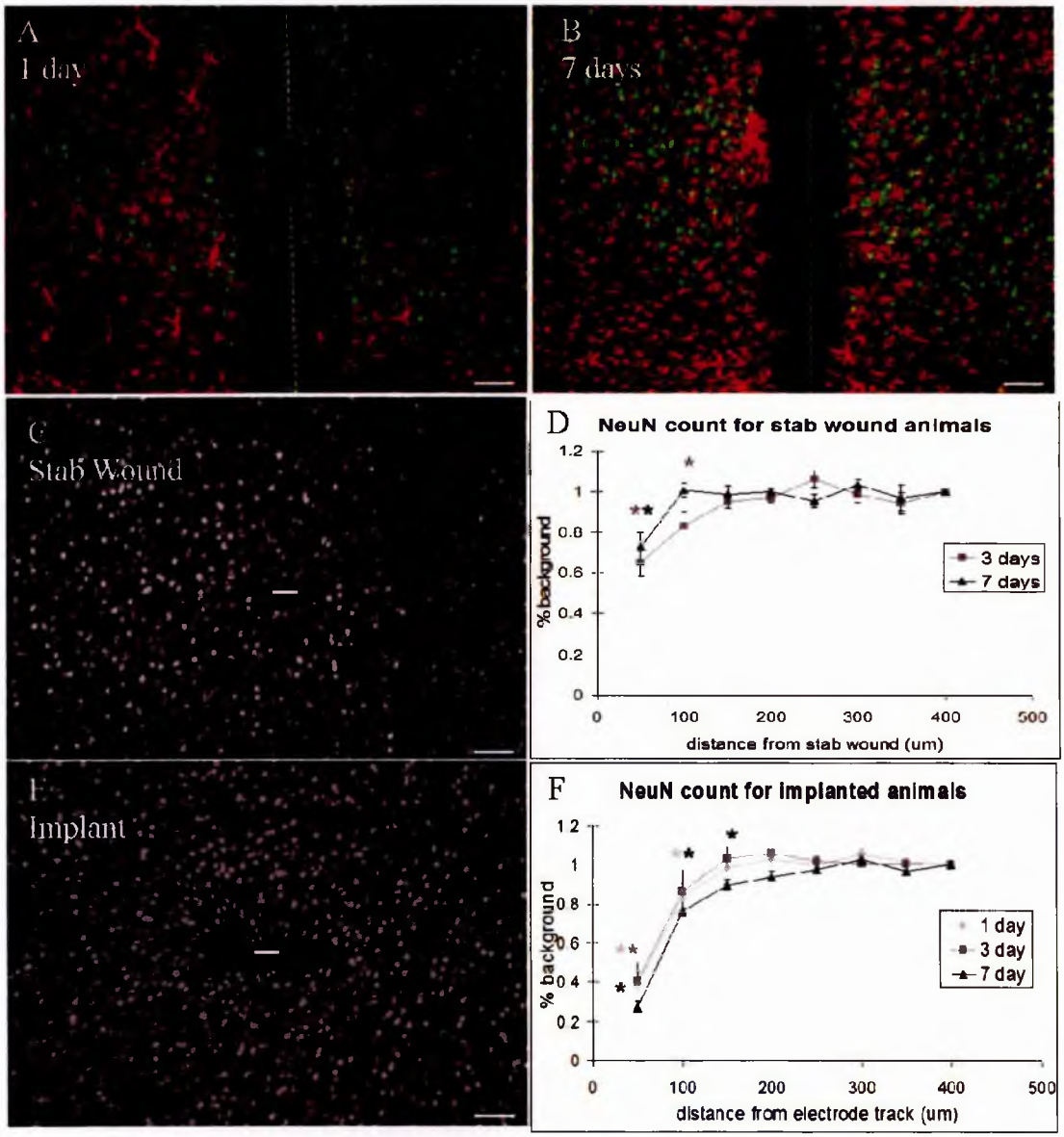

Figure 12. Neuronal cell loss increased in implanted animals, secondary loss. A and B) Representative coronal sections for NeuN (green) and GFAP (red). A) In the least reactive cases, neuronal nuclei were decreased within the first 50 μm from the implant but were found in an area where all astrocytes were absent. B) Neurons were found at or behind the hypertrophied astrocytes at 7 days. C) Representative horizontal NeuN image for stab wound animals. D) Line profile data for stab wound animals. Average loss was 30% from background within the first 50 μm from the wound. Loss at 3 day was significant from 0-100 μm, and from 0-50 μm at 7 days. E) Representative NeuN image for implanted animals. F) Line profile data for implanted animals. Average loss within the first 50 μm from the implant site was decreased by 70% compared to background values. The loss at 1 day was significant from 0-100 μm, which increased at 7 days to 0-150 μm from the electrode track. Asterisk denotes significant compared to background, t-test $p<0.05$. Error bars are SEM. Electrode track represented by dashed line. Scale bar = 100 μm.

values previously reported at 12 weeks for Michigan electrodes implanted into rat cortex (Biran et al., 2005). While the density of neuronal bodies within 50 μm was not significantly different among implanted animals at each time point, the distance, or zone of neuronal loss increased over time. Neuronal loss was significant from background measures to a distance of 100 μm at 1 and 3 days and to a distance of 150 μm from the implant site at 7 days, suggesting secondary delayed neuronal loss event, (Figure 12).

The average decrease in neuronal density within the first 50 μm of the stab wound was about 30% from background, less than the average 70% loss for implanted animals. On average, implanted animals had about a 40% increase in neuronal loss when compared to stab wound animals. This increased loss corresponds to a decrease from 3-4 neurons within the recording zone to only 1-2 neurons present within the first 0-50 μm from the electrode due to the presence of the foreign body. The decrease in neurons within the recording zone can decrease the chance of obtaining a reliable single-unit recording. At 3 days postinjury, the zone of neuronal loss was significant to a distance of 100 μm. Loss at 7 days was significant from 0-50 μm from the stab wound.

Antigen profile curves for NeuN, overlaid with GFAP and ED-1 profiles, illustrate the clearance of the marker at the implant site (Figure 13). At 1 and 3 days postimplantation, the intensity of the NeuN antigen was increased adjacent to the implant track, which closely corresponds to ED-1 reactivity profiles at the same time points. By day 7, there was a decrease in the NeuN antigen intensity, which follows the trend of GFAP loss. The increased intensity of NeuN at 1 and 3 days was not due

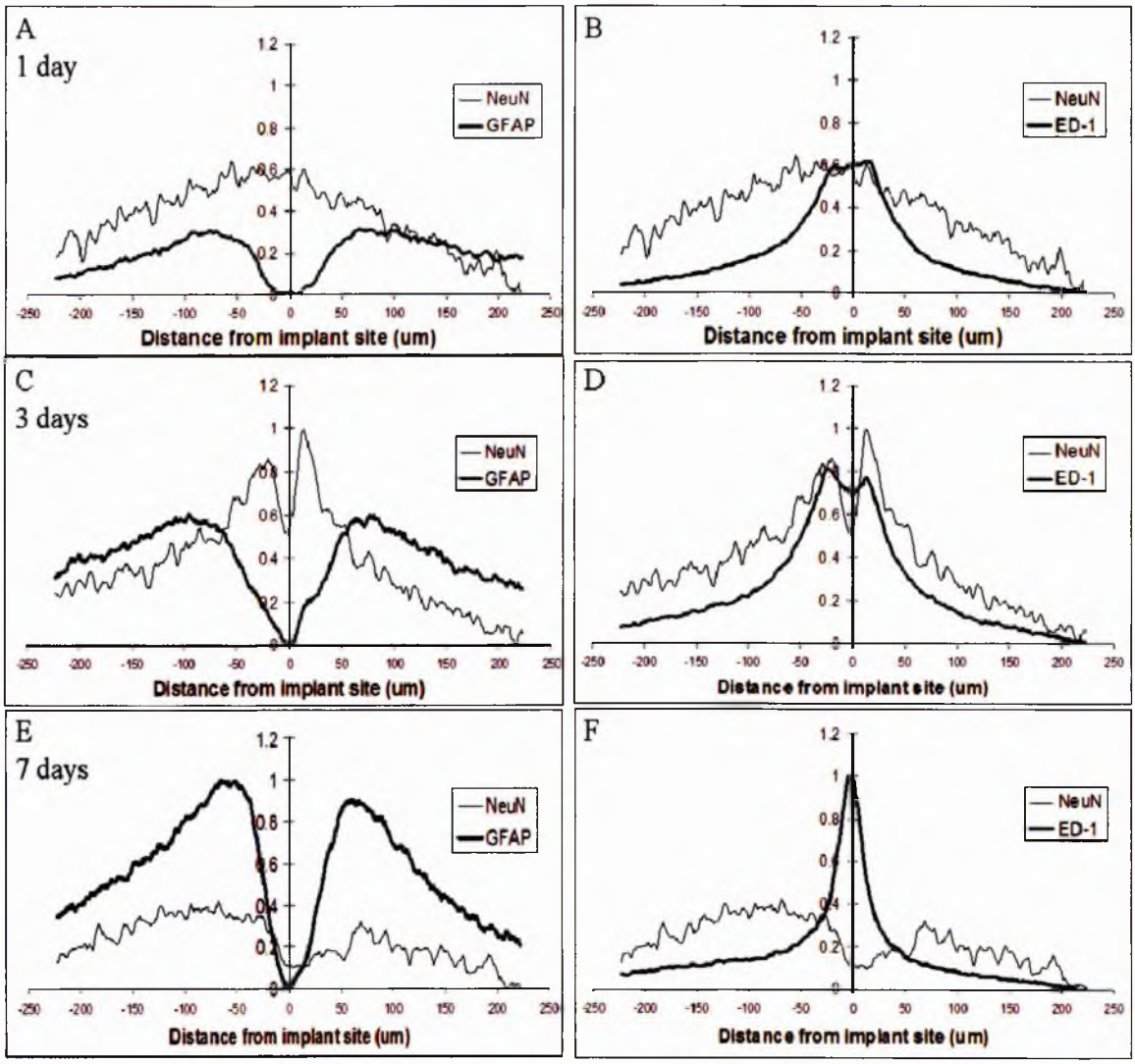

Figure 13. Antigen profile curves for NeuN overlaid with GFAP (A, C, E) and ED-1 (B, D, F) as a function of time. A and B) At 1 day postimplantation, the intensity of the NeuN antigen was increased adjacent to the implant site, with a peak intensity equal to that of ED-1, B. Counts of neuronal soma adjacent to the implant site demonstrated a loss of neurons within the first 50 μm, comparable to the zone of absent astrocytes, A. C and D) By 3 days, NeuN intensity was still increased next to the implant site, and again closely followed the ED-1 intensity trend. E and F) By day 7, NeuN antigen intensity was decreased adjacent to the implant site, following the trend of astrocyte loss, E, and was inversely related to ED-1 expression, F.

to an increase in cell number; the density of neuronal nuclei is decreased adjacent to the electrode track indicated by counts of $NeuN^+$ cell bodies as a function of distance from the implant site.

The high degree of variability among experimental animals was evident by the amount hemorrhaging at the surface of the brain as well as by cell-specific markers throughout the depth of the cortex. Visual observation of tissue sections from implanted animals suggested that the variability of the cellular response surrounding the electrode track at 7 days was less compared to that observed at 1 or 3 days postimplantation. To quantitatively measure this observation, the averaged variability of each marker, expressed as the standard deviations among all animals, were analyzed as a function of time. While the total average variability of each marker did not change from 1 to 7 days, the variability of the ED-1 and GFAP antigens within the first 100 μm of the implant had decreased over time (data not shown).

CHAPTER 4

DISCUSSION

The use of recording electrodes in chronic applications for brain-machine interfaces relies on their ability to maintain a stable interface between functioning nervous tissue and the electrode, specifically with the recording site. It is important to characterize that interface, including how the adjacent tissue changes over time. While the chronic response has been well defined (Linell, 1928; Drapiewski et al., 1943; Collias and Manuelidis, 1957; Dymond et al., 1970; Schultz and Willey, 1976; Stensaas and Stensaas, 1976; Stensaas and Stensaas, 1978; Agnew et al., 1986; Turner et al., 1999; Szarowski et al., 2003; Biran et al., 2005), few have studied the early events in the foreign body response. In this study we demonstrated that, in response to implanted Michigan-style microelectrode arrays, remodeling of glial and neuronal populations occurs during the early stages of the foreign body response, which is distinct from early wound healing events in the CNS. The foreign body response consisted of an exacerbated macrophage response correlated to a loss of astrocytes immediately adjacent to the electrodes, a hypertrophy of remaining astrocytes, and about a 40% increase in the loss of neurons within the recording zone.

Evidence of hemorrhagic responses on the surface of explanted rat brains illustrates the high degree of variability that exists between animals and the remodeling that occurs during the first 7 days postimplantation. There was a large

range of bleeding and necrosis on the surface of explanted brains and within the superficial cortical layers that greatly decreased over time, where the average response at 7 days was similar to brains explanted at later time points or uninjured brains. In general, glial populations become activated at the electrode track by 1 day with respect to macrophages, and from 3-7 days for astrocytes. An apparent increase in total cell density was qualitatively observed with DAPI staining at the interface at 3 and 7 days, either due to migration alone or also due to hyperplasia of glial populations. In the least reactive cases, $ED1^{+}$ macrophages were present both attached to retrieved electrodes and in the tissue immediately adjacent to the implant site by 24 hours in both stab wound and experimental animals. Activated macrophages were also observed in surrounding tissue at 1 and 3 days, which may be due to extravasation of blood-borne macrophages and migration toward the implant or due to vascular damage, for example. Astrocytes in the surrounding tissue began to upregulate expression of GFAP by 1 day. Astrocytes were increasingly hypertrophic and formed the early stages of an astroglial scar by 7 days. Evidence from this study suggests that astrocytes are sensitive to early events in the foreign body response, as a clear zone of astrocytes loss was found adjacent to the electrode track for all implanted animals while stab wound animals showed little to no loss of astrocytes at the electrode-tissue interface. In implanted animals, neuronal loss was significantly different from loss in stab wound animals to a distance of 100 μm from the electrode track, with an increased loss of about 40% compared to the stab wound within the first 50 μm. Further, the area of neuronal cell loss increased from 100 μm at day 1 to

150 μm at day 7, suggesting that secondary neuronal cell death is also part of the early phase of the foreign body response.

Glial reactivity

In this study, the macrophage response involved activation and migration to the stab wound or electrode track. We observed an increased macrophage response for animals with indwelling electrodes, which is consistent with previous findings that the macrophage response to brain injury is proportional to the severity of the insult (Kreutzberg et al., 1996; Fujita et al., 1998; Carbonell et al., 2005). Animals with indwelling electrodes may present a more severe injury type due to the persistent inflammatory response at the site of injury, which does not occur in response to a penetrating injury alone. Recruitment of blood-borne macrophages may be a response to the release of cytokines from macrophages at the interface. Activated macrophages have the ability to initiate an inflammatory response by the secretion of cytokines as well as phagocytose (Becher et al., 2000S). Active phagocytosis was evident by the clearance of blood products and NeuN antigen at the interface. Cytokines released by macrophages at the interface, such as TNF-α and interleukins are proinflammatory and may be cytotoxic, affecting both adjacent actrocytes and neurons (Bezzi and Volterra, 2001). Macrophages attached to explanted electrodes have also been shown to release cytokines (Biran et al., 2005). The chemokine system that is initiated, including those systems that promote or resist immunoregulation, tissue repair, and remodeling, is related to macrophage activation and polarization (Manatovani et al., 2004). Further, frustrated phagocytosis may occur with the continued presence of an implanted, nondegradable material, leading to the formation of multiucleated cells

(Stensaas and Stensaas, 1976; Stensaas and Stensaas, 1978); which together with macrophages adhering to indwelling electrodes may encourage an increased, unresolved macrophage response at the electrode-tissue interface.

The astrocyte response in implanted animals was characterized by two phenomena: a decrease in astrocytes adjacent to the electrode track, and a hypertrophy of remaining astrocytes that formed the early stages of an astroglial scar at the perimeter of the zone of loss. This dual event was also observed in response to LPS-induced neuroinflammation in the rat brain (Ambrosini et al., 2005). Likewise, a loss of astrocytes within 15 minutes to 24 hours after mechanical damage was observed *in vitro* (Engel et al., 2005). Loss of astrocytes may be due to ischemic or inflammatory events. Astrocyte swelling has been observed as a result of cytotoxic edema and K^+ ion uptake to maintain extracellular homeostatsis (Bullock et al., 1991). Further, the presence of activated macrophages and the cytokines they secrete may affect the function and viability of astrocytes within a diffusion-limited area (Gareth et al., 1999; Bezzi and Voltera, 2001; Polikov et al., 2006). However, ischemia and the presence of activated macrophages are also a part of the mechanical damage inflicted in stab wound animals, which showed no loss of astrocytes adjacent to the wound site. Further work is needed to elucidate the mechanisms of astrocyte loss that occurs during the foreign body response.

The formation of an astroglial scar is the result of high concentration of hypertrophied astrocytes adjacent to the implant site. Evidence of hyperplasia of astrocytes by 7 days is supported by studies which observed GFAP precursor cells ($GFAP^-$/$vimentin^+$) that migrated to the wound site by 24-48 hours, incorporated

BrdU, and became $GFAP^+$ by 7 days (Szwaroski et al., 2003; Polikov et al., 2006). In addition, hypertrophied astrocytes were also found in stab wound animals. However, this astroglial response has been found to dissipate after several months in longer-term stab wound experiments (Rousche et al., 2001; Csicsvari et al., 2003; Biran et al., 2005).

Neurodegeneration

Significant neuronal loss was observed within the first 0-100 μm from the electrode track in implanted animals, and from 0-50 μm in stab wound animals. In addition, neuronal loss within the first 0-100 μm from the implant was not found to be significant in stab wound animals after 2 and 4 weeks (Biran et al., 2005). The acute neuronal loss events that were observed at 1 and 3 days are supported by experimental traumatic brain injuries to rat cortex that demonstrate an initial neuronal injury occurring as early as 10 minutes (Hicks et al., 1996) and continuing from 1-3 days (Dietrich et al., 1994; Liu et al., 1997; Sato et al., 2001). An increase in the area of neuronal loss was also found to extend 0-150 μm from the electrode track at 7 days postimplantation. Delayed neuronal death has also been observed in response to traumatic injury and LPS-induced neuroinflammation (Liu et al., 1997; Sato et al., 2001; Ambrosini et al., 2005).

The mechanisms of neuronal degeneration, including apoptosis and necrosis, have been described in detail (Crowe et al., 1997; Martin et al., 1998; Heidenreich, 2003). Neuronal loss due to the mechanical damage incurred during implantation, which results in ischemia when vasculature is disrupted, is generally considered a necrotic event. However, some studies have found apoptotic neurons from 24 hours to 1 week

following injury (Conti et al., 1998). The mechanism of delayed neuronal death is mostly by apoptosis, although it has been proposed that injured neurons in the adult CNS may be less capable of classic apoptosis resulting instead in an apoptosis-necrosis hybrid method (Martin et al., 1998). Microcircuits in the CNS are composed of anatomically and functionally distinct neuron populations and some neuronal populations may be more vulnerable to different types of injury (Markram et al., 2005), although the degree of neuronal loss was not found to change with a function of depth and the changing neuron populations throughout the cortex (Williamson, 2006). It is important to determine the mechanism of cell death as antiapoptotic therapies might be useful in preventing some secondary neuronal loss. While neurogenesis in the adult brain is generally underappreciated, one study found that after ischemia, neuroblasts generated in the subventricular zone continually migrated into the striatum for up to 4 months after injury. The neuroblasts either differentiated into neurons or died by apoptosis (Thored et al., 2006). However, neurogenesis has not been found in the zone of loss surrounding indwelling electrodes. The cytotoxic environment created by activated macrophages that persist attached to the electrodes and at the interface may discourage the recruitment, differentiation, and/or survival of neuroblasts.

Neuron/glial plasticity

Changes in glial reactivity in response to the presence of a foreign body, namely an increase in macrophages and a loss of astrocytes at the interface, is likely responsible for the increased neuronal loss in implanted animals. Neuron/glia interactions are vital in maintaining brain homeostasis, and the loss of astroglial cells

may adversely affect the survival of neurons after brain injury and persisting during chronic inflammatory events. In uninjured tissue, astrocyte processes are intimately apposed to neuronal synapses in neural networks within various areas of the brain (Bezzi and Voltera, 2001). Neuron-astrocyte signaling, whereby astrocytes upregulate intracellular calcium concentrations in response to neurotransmitter release, may be perturbed by the release of cytotoxic cytokines from macrophages. Deranged astrocyte-to-neuron signaling has been found to lead to reduced viability of the surrounding neurons (Bezzi and Voltera, 2001). Macrophages may be responsible in part for the disruption in the astrocyte/neuron relationship. *In vitro* experiments have shown that the presence of activated macrophages and microglia were detrimental to the survival of neurons after 24 hours to 3 days, even in the presence of astrocytes (Bullock et al., 1991; Polikov et al., 2006). As mentioned above, cytokines known to be released by macrophages negatively affect the signaling ability of astrocytes. In addiction, calcium-dependent glutamate release has been demonstrated by astrocytes exposed to TNF-α (Bezzi and Voltera, 2001). Another direct mechanism of glial participation in neurodegeneration may occur when pro-apoptotic astrocytes communicate to surrounding viable neuronal cells though gap junctions, as reported for ischemic cortical regions (Bezzi and Voltera, 2001). Neurodegeneration may also be a result of abandonment by astrocytes that migrate to the site of injury.

Many studies demonstrate the response of glial and neuronal populations to injury, and it is unclear to what degree neuronal death, the nature of neuronal network plasticity, and the astroglial response itself, which can increase impedance (Liu et al., 1999), plays a role in the inconsistent recording performances of implanted

microelectrodes. Local field potentials, which sample a larger population of neurons, may prove more reliable in maintaining usable signals for neuroprosthetic devices (Pesaran et al., 2002).

Future work

While the early foreign body events may dictate the longterm inflammatory phenotype that is characteristic of CNS implants like the Michigan silicon electrode array, the reason for signal degeneration in chronic implants remains elusive. One study used SEM to visualize structural modifications of an implanted microwire electrode that were responsible, at least in part, for an inconsistent recording ability (Sanchez et al., 2006). New designs for microelectrodes use bioactive approaches such as neurotrophic factors and microfluidic channels that can release therapeutic agents into surrounding nervous tissue to increased integration of implanted electrodes. The cone, or neurotrophic electrode, is a newer design that has been implanted into human patients (Kennedy et al., 2000). The cone electrode consists of a hollow electrode tip with wires and neurotrophic factors that encourage growth of neural tissue into the tip and through both ends.

In addition, pharmacological agents may be developed to attenuate tissue responses in an effort to stabilize the tissue interface. For example, dexamethasone is a synthetic glucocorticoid effective in treating many anti-inflammatory responses that has been found to attenuate the astrogliotic response surrounding implanted microelectrodes (Shain et al., 2003). Minocycline is a broad spectrum tetracycline antibiotic that may attenuate the macrophage response when administered to implanted animals. In an ongoing study minocycline was administered by daily

injection for two weeks after implantation (Chen, unpublished data). The macrophage response was decreased compared to saline-injected controls; however the systemic inflammatory response due to the injections exacerbated the overall tissue response surrounding indwelling electrodes. Pharmacological approaches are likely to prove effective in decreasing the difference between the tissue reactivity to the presence of the foreign body and to the initial injury during implantation.

In parallel to improving the electrode-tissue interface, new technology must be continually developed. The use of on-chip buffering, amplification, and signal multiplexing have been proposed to reduce crosstalk, signal noise, and the number of external leads (Najafi and Wise, 1986; Bai and Wise, 2001). Ultimately, wireless technology for amplifying and transmitting signals must be developed to progress the use of invasive microelectrodes in chronically implanted neuroprosthetic devices.

Conclusions

This study demonstrated that remodeling of glial and neuronal populations occurs during the early foreign body response, which that is greatly increased from the remodeling events that occur due to the initial mechanical damage alone. Macrophages became activated, accumulate at the site of injury, and adhere to electrodes within the first 24 hours postimplantation. The astrocytes response consisted of an early astrocytes loss and hypertrophy of remaining astrocytes from 3 to 7 days postimplantation. This glial response was accompanied by a decrease in the density of neuronal soma immediately surrounding the implant by 1 day and increasing at 7 days. These events were exaggerated in implanted animals compared to stab wound animals, suggesting that the foreign body response dictates the early

tissue response to implanted Michigan-style microelectrodes. The increased macrophage response may be the key to the astrocytes loss and increased neuronal loss within the recording zone; however, the mechanism and regulation of the switch from normal wound healing events in the CNS to a chronic inflammatory response needs to be further investigated. Future studies may determine whether it is possible to use pharmacological methods, for example, to modulate these early events in order to decrease the amount of neuronal loss within the recording zone, thereby potentially prolonging the recording ability of implanted microelectrodes and increasing their clinical use in brain-machine interfaces.

REFERENCES

(2001). Deep-brain stimulation of the subthalamic nucleus or the pars interna of the globus pallidus in Parkinson's disease. N Engl J Med 345, 956-963.

Agnew, W. F., Yuen, T. G., McCreery, D. B., and Bullara, L. A. (1986). Histopathologic evaluation of prolonged intracortical electrical stimulation. Exp Neurol 92, 162-185.

Ambrosini, A., Louin, G., et al. (2005). Characterization of a rat model to study acute neuroinflammation on histopathological, biochemical and functional outcomes. J Neurosci Methods 144, 183-91.

Bai, Q., and Wise, K. D. (2001). Single-unit neural recording with active microelectrode arrays. IEEE Trans Biomed Eng 48, 911-920.

Bezzi, P., and Volterra, A. (2001). A neuron-glia signalling network in the active brain. Curr Opin Neurobiol 11, 387-394.

Biran, R., Martin, D. C., and Tresco, P. A. (2005). Neuronal cell loss accompanies the brain tissue response to chronically implanted silicon microelectrode arrays. Exp Neurol 195, 115-126.

Bramlett, H. M., and Dietrich, W. D. (2002). Quantitative structural changes in white and gray matter 1 year following traumatic brain injury in rats. Acta Neuropathol (Berl) 103, 607-614.

Bullock, R., Maxwell, W. L., Graham, D. I., Teasdale, G. M., and Adams, J. H. (1991). Glial swelling following human cerebral contusion: an ultrastructural study. J Neurol Neurosurg Psychiatry 54, 427-434.

Buzsaki, G., and Chrobak, J. J. (2005). Synaptic plasticity and self-organization in the hippocampus. Nat Neurosci 8, 1418-1420.

Carbonell, W. S., Murase, S., Horwitz, A. F., and Mandell, J. W. (2005). Migration of perilesional microglia after focal brain injury and modulation by CC chemokine receptor 5: an in situ time-lapse confocal imaging study. J Neurosci 25, 7040-7047.

Collias, J. C., and Manuelidis, E. E. (1957). Histopathological changes produced by implanted electrodes in cat brains; comparison with histopathological changes in human and experimental puncture wounds. J Neurosurg 14, 302-328.

Conti, A. C., Raghupathi, R., Trojanowski, J. Q., and McIntosh, T. K. (1998). Experimental brain injury induces regionally distinct apoptosis during the acute and delayed post-traumatic period. J Neurosci 18, 5663-5672.

Copeland, B. J., and Pillsbury, H. C., 3rd (2004). Cochlear implantation for the treatment of deafness. Annu Rev Med 55, 157-167.

Crowe, M. J., Bresnahan, J. C., Shuman, S. L., Masters, J. N., and Beattie, M. S. (1997). Apoptosis and delayed degeneration after spinal cord injury in rats and monkeys. Nat Med 3, 73-76.

Csicsvari, J., Henze, D. A., Jamieson, B., Harris, K. D., Sirota, A., Bartho, P., Wise, K. D., and Buzsaki, G. (2003). Massively parallel recording of unit and local field potentials with silicon-based electrodes. J Neurophysiol 90, 1314-1323.

Dhillon, G. S., and Horch, K. W. (2005). Direct neural sensory feedback and control of a prosthetic arm. IEEE Trans Neural Syst Rehabil Eng 13, 468-472.

Donoghue, J. P. (2002). Connecting cortex to machines: recent advances in brain interfaces. Nat Neurosci 5 Suppl, 1085-1088.

Drapiewski, J. B., AH; Kernohan, JW (1943). The healing wounds of the brain. AMERICAN JOURNAL OF CLINICAL PATHOLOGY, 333-348.

Dymond, A. M., Kaechele, L. E., Jurist, J. M., and Crandall, P. H. (1970). Brain tissue reaction to some chronically implanted metals. J Neurosurg 33, 574-580.

Eaton, K.P. and C.S. Henriquez. (2005). Confounded spikes generated by synchrony within neural tissue models. Neurocomputing 65, 851-875.

Edell, D. J., Toi, V. V., McNeil, V. M., and Clark, L. D. (1992). Factors influencing the biocompatibility of insertable silicon microshafts in cerebral cortex. IEEE Trans Biomed Eng 39, 635-643.

Engel, D. C., Slemmer, J. E., Vlug, A. S., Maas, A. I., and Weber, J. T. (2005). Combined effects of mechanical and ischemic injury to cortical cells: secondary ischemia increases damage and decreases effects of neuroprotective agents. Neuropharmacology 49, 985-995.

Evarts, E. V. (1966). Pyramidal tract activity associated with a conditioned hand movement in the monkey. J Neurophysiol 29, 1011-1027.

Farah, C. A., Liazoghli, D., Perreault, S., Desjardins, M., Guimont, A., Anton, A., Lauzon, M., Kreibich, G., Paiement, J., and Leclerc, N. (2005). Interaction of microtubule-associated protein-2 and p63: a new link between microtubules and rough endoplasmic reticulum membranes in neurons. J Biol Chem 280, 9439-9449.

Fitch, M. T., Doller, C., Combs, C. K., Landreth, G. E., and Silver, J. (1999). Cellular and molecular mechanisms of glial scarring and progressive cavitation: in vivo and in vitro analysis of inflammation-induced secondary injury after CNS trauma. J Neurosci 19, 8182-8198.

Friehs, G. M., Zerris, V. A., Ojakangas, C. L., Fellows, M. R., and Donoghue, J. P. (2004). Brain-machine and brain-computer interfaces. Stroke 35, 2702-2705.

Fujita, T., Yoshimine, T., Maruno, M., and Hayakawa, T. (1998). Cellular dynamics of macrophages and microglial cells in reaction to stab wounds in rat cerebral cortex. Acta Neurochir (Wien) 140, 275-279.

Gareth, R. S., E; Suadicani, SO; liu, js; charles, pc; sunhee, cl; spray, dc; brosnan, cf (1999). IL-1B differentially regulates calcium wave propagation between primary human fetal astrocytes via pathways involving P2 receptors and gap junction channels. proc natl acad sci USA 96, 11613-11618.

Gavrieli, Y., Sherman, Y., and Ben-Sasson, S. A. (1992). Identification of programmed cell death in situ via specific labeling of nuclear DNA fragmentation. J Cell Biol 119, 493-501.

Griffith, R. W., and Humphrey, D. R. (2006). Long-term gliosis around chronically implanted platinum electrodes in the Rhesus macaque motor cortex. Neurosci Lett 406, 81-86.

Grillner, S., Markram, H., De Schutter, E., Silberberg, G., and LeBeau, F. E. (2005). Microcircuits in action--from CPGs to neocortex. Trends Neurosci 28, 525-533.

Harris, K. D., Csicsvari, J., Hirase, H., Dragoi, G., and Buzsaki, G. (2003). Organization of cell assemblies in the hippocampus. Nature 424, 552-556.

Heidenreich, K. A. (2003). Molecular mechanisms of neuronal cell death. Ann N Y Acad Sci 991, 237-250.

Henze, D. A., Borhegyi, Z., Csicsvari, J., Mamiya, A., Harris, K. D., and Buzsaki, G. (2000). Intracellular features predicted by extracellular recordings in the hippocampus in vivo. J Neurophysiol 84, 390-400.

Hochberg, L. R., Serruya, M. D., Friehs, G. M., Mukand, J. A., Saleh, M., Caplan, A. H., Branner, A., Chen, D., Penn, R. D., and Donoghue, J. P. (2006). Neuronal

ensemble control of prosthetic devices by a human with tetraplegia. Nature 442, 164-171.

Humphrey, D. R., Schmidt, E. M., and Thompson, W. D. (1970). Predicting measures of motor performance from multiple cortical spike trains. Science 170, 758-762.

Kennedy, P. R., Bakay, R. A., Moore, M. M., Adams, K., and Goldwaithe, J. (2000). Direct control of a computer from the human central nervous system. IEEE Trans Rehabil Eng 8, 198-202.

Kim, Y. T., Hitchcock, R. W., Bridge, M. J., and Tresco, P. A. (2004). Chronic response of adult rat brain tissue to implants anchored to the skull. Biomaterials 25, 2229-2237.

Kipke, D. R., Vetter, R. J., Williams, J. C., and Hetke, J. F. (2003). Silicon-substrate intracortical microelectrode arrays for long-term recording of neuronal spike activity in cerebral cortex. IEEE Trans Neural Syst Rehabil Eng 11, 151-155.

Linell, E. (1929). The histology of neuroglial changes followingn cerebral trauma. Archs neurol Psych, 926-948.

Liu, X. Z., Xu, X. M., Hu, R., Du, C., Zhang, S. X., McDonald, J. W., Dong, H. X., Wu, Y. J., Fan, G. S., Jacquin, M. F., et al. (1997). Neuronal and glial apoptosis after traumatic spinal cord injury. J Neurosci 17, 5395-5406.

Liu, X., McCreery, D. B., Carter, R. R., Bullara, L. A., Yuen, T. G., and Agnew, W. F. (1999). Stability of the interface between neural tissue and chronically implanted intracortical microelectrodes. IEEE Trans Rehabil Eng 7, 315-326.

Liu, X., McCreery, D. B., Bullara, L. A., and Agnew, W. F. (2006). Evaluation of the stability of intracortical microelectrode arrays. IEEE Trans Neural Syst Rehabil Eng 14, 91-100.

Mantovani, A., Sica, A., Sozzani, S., Allavena, P., Vecchi, A., and Locati, M. (2004). The chemokine system in diverse forms of macrophage activation and polarization. Trends Immunol 25, 677-686.

Marg, E., and Adams, J. E. (1967). Indwelling multiple micro-electrodes in the brain. Electroencephalogr Clin Neurophysiol 23, 277-280.

Martin, L. J., Al-Abdulla, N. A., Brambrink, A. M., Kirsch, J. R., Sieber, F. E., and Portera-Cailliau, C. (1998). Neurodegeneration in excitotoxicity, global cerebral ischemia, and target deprivation: A perspective on the contributions of apoptosis and necrosis. Brain Res Bull 46, 281-309.

Martinez Santiesteban, F. M., Swanson, S. D., Noll, D. C., and Anderson, D. J. (2006). Magnetic resonance compatibility of multichannel silicon microelectrode systems for neural recording and stimulation: design criteria, tests, and recommendations. IEEE Trans Biomed Eng 53, 547-558.

Maynard, E. M., Hatsopoulos, N. G., Ojakangas, C. L., Acuna, B. D., Sanes, J. N., Normann, R. A., and Donoghue, J. P. (1999). Neuronal interactions improve cortical population coding of movement direction. J Neurosci 19, 8083-8093.

Moxon, K. A., Leiser, S. C., Gerhardt, G. A., Barbee, K. A., and Chapin, J. K. (2004). Ceramic-based multisite electrode arrays for chronic single-neuron recording. IEEE Trans Biomed Eng 51, 647-656.

Najafi, K. W., KD (1986). An implantable multielectrode array with on-chip signal processing. IEEE Journal of solid-state circuits 21, 1035-1044.

Nicolelis, M. A., Dimitrov, D., Carmena, J. M., Crist, R., Lehew, G., Kralik, J. D., and Wise, S. P. (2003). Chronic, multisite, multielectrode recordings in macaque monkeys. Proc Natl Acad Sci U S A 100, 11041-11046.

Nimmerjahn, A., Kirchhoff, F., and Helmchen, F. (2005). Resting microglial cells are highly dynamic surveillants of brain parenchyma in vivo. Science 308, 1314-1318.

Palmer, C. (1978). A microwire technique for recording single neurons in unrestrained animals. Brain Res Bull 3, 285-289.

Pesaran, B., Pezaris, J. S., Sahani, M., Mitra, P. P., and Andersen, R. A. (2002). Temporal structure in neuronal activity during working memory in macaque parietal cortex. Nat Neurosci 5, 805-811.

Polikov, V. S., Block, M. L., Fellous, J. M., Hong, J. S., and Reichert, W. M. (2006). In vitro model of glial scarring around neuroelectrodes chronically implanted in the CNS. Biomaterials 27, 5368-5376.

Retterer, S. T., Smith, K. L., Bjornsson, C. S., Neeves, K. B., Spence, A. J., Turner, J. N., Shain, W., and Isaacson, M. S. (2004). Model neural prostheses with integrated microfluidics: a potential intervention strategy for controlling reactive cell and tissue responses. IEEE Trans Biomed Eng 51, 2063-2073.

Rodriguez-Paez, A. C., Brunschwig, J. P., and Bramlett, H. M. (2005). Light and electron microscopic assessment of progressive atrophy following moderate traumatic brain injury in the rat. Acta Neuropathol (Berl) 109, 603-616.

Rousche, P. J., and Normann, R. A. (1998). Chronic recording capability of the Utah Intracortical Electrode Array in cat sensory cortex. J Neurosci Methods 82, 1-15.

Sanchez, J. C., Alba, N., Nishida, T., Batich, C., and Carney, P. R. (2006). Structural modifications in chronic microwire electrodes for cortical neuroprosthetics: a case study. IEEE Trans Neural Syst Rehabil Eng 14, 217-221.

Sato, M., Chang, E., Igarashi, T., and Noble, L. J. (2001). Neuronal injury and loss after traumatic brain injury: time course and regional variability. Brain Res 917, 45-54.

Schmidt, E. M., Bak, M. J., and McIntosh, J. S. (1976). Long-term chronic recording from cortical neurons. Exp Neurol 52, 496-506.

Schultz, R. L., and Willey, T. J. (1976). The ultrastructure of the sheath around chronically implanted electrodes in brain. J Neurocytol 5, 621-642.

Schwartz, M., Butovsky, O., Bruck, W., and Hanisch, U. K. (2006). Microglial phenotype: is the commitment reversible? Trends Neurosci 29, 68-74.

Serruya, M. D., Hatsopoulos, N. G., Paninski, L., Fellows, M. R., and Donoghue, J. P. (2002). Instant neural control of a movement signal. Nature 416, 141-142.

Shain, W., Spataro, L., Dilgen, J., Haverstick, K., Retterer, S., Isaacson, M., Saltzman, M., and Turner, J. N. (2003). Controlling cellular reactive responses around neural prosthetic devices using peripheral and local intervention strategies. IEEE Trans Neural Syst Rehabil Eng 11, 186-188.

Shoham, S., Halgren, E., Maynard, E. M., and Normann, R. A. (2001). Motor-cortical activity in tetraplegics. Nature 413, 793.

Stence, N., Waite, M., and Dailey, M. E. (2001). Dynamics of microglial activation: a confocal time-lapse analysis in hippocampal slices. Glia 33, 256-266.

Stensaas, S. S., and Stensaas, L. J. (1976). The reaction of the cerebral cortex to chronically implanted plastic needles. Acta Neuropathol (Berl) 35, 187-203.

Stensaas, S. S., and Stensaas, L. J. (1978). Histopathological evaluation of materials implanted in the cerebral cortex. Acta Neuropathol (Berl) 41, 145-155.

Szarowski, D. H., Andersen, M. D., Retterer, S., Spence, A. J., Isaacson, M., Craighead, H. G., Turner, J. N., and Shain, W. (2003). Brain responses to micro-machined silicon devices. Brain Res 983, 23-35.

Taylor, D. M., Tillery, S. I., and Schwartz, A. B. (2002). Direct cortical control of 3D neuroprosthetic devices. Science 296, 1829-1832.

Thored, P., Arvidsson, A., Cacci, E., Ahlenius, H., Kallur, T., Darsalia, V., Ekdahl, C. T., Kokaia, Z., and Lindvall, O. (2006). Persistent production of neurons from adult brain stem cells during recovery after stroke. Stem Cells 24, 739-747.

Turner, J. N., Shain, W., Szarowski, D. H., Andersen, M., Martins, S., Isaacson, M., and Craighead, H. (1999). Cerebral astrocyte response to micromachined silicon implants. Exp Neurol 156, 33-49.

Wessberg, J., Stambaugh, C. R., Kralik, J. D., Beck, P. D., Laubach, M., Chapin, J. K., Kim, J., Biggs, S. J., Srinivasan, M. A., and Nicolelis, M. A. (2000). Real-time prediction of hand trajectory by ensembles of cortical neurons in primates. Nature 408, 361-365.

Wieloch, T., and Nikolich, K. (2006). Mechanisms of neural plasticity following brain injury. Curr Opin Neurobiol 16, 258-264.

Williamson, T. (2006). "Characterization of tissue reactivity to microelectrode arrays as a function of depth in the rat cerebral cortex." Master's Thesis.

Wolpaw, J. R., McFarland, D. J., and Vaughan, T. M. (2000). Brain-computer interface research at the Wadsworth Center. IEEE Trans Rehabil Eng 8, 222-226.